Time-Series Prediction of the Offshore and Onshore Wind Profiles using the Autoencoding Models: Lidar and Meteorological Measurements Based

ZACCHEUS O. OLAOFE[1,2,*]

[1] ZakkWea Energy (ZWE), Lagos, 102212, Nigeria
[2] University of Cape Town, Rondebosch, Cape Town, 7701, South Africa
*Corresponding author email: zakky201@gmail.com

The development of the reliable forecast model plays a vital role in describing the variability of the time-series (very- to long-term) wind profiles of a particular climatic zone. In this paper, the time-series multivariate forecasts and analysis of the air temperature, CNR, offshore/onshore wind profiles from the lidar and meteorological measurements based on 2–autoencoding architectures are presented. The historical datasets (lidar measurements and meteorological masts) of the selected multivariables at 5– and 10–minute intervals are collected. Two autoencoding architectures (Conv2D and GRU encoding-decoding networks) in an unsupervised predictive operation are used for the time-series multivariable forecasting (1-288 horizons) and analysis of the: wind speed and wind direction, sectorwise windrose, CNR and prevailing air temperature. At the period of 48 timesteps, the time-series wind speed and direction variations are analyzed in determining the measurement data height with the steadiest wind flows for optimal loading of the large-scale wind turbine. Studied finding results of the offshore wind profiles at different heights revealed the existence of a steadiest wind flow at 128.8 m height but driven by the atmospheric effects. Also, the experimental findings revealed that the dominant wind flows of the onshore heights (10-20m) are impacted by the local surface irregularities and atmospheric effects. Finally, the autoencoders performance is reported for the experimental offshore and onshore wind flow for different heights with and without the feature noise removal. Upon validation and evaluation of the autoencoders with actual model, the GRU autoencoder produces better forecast of the time-series of the onshore station multivariables, while the Conv2D and GRU architectures are needful for the predictions of the offshore station multivariables. The proposed model architectures clearly shown to be an essential forecast tool in providing a more robust wind resource estimates from the time-series predictions of the multivariable input sequences at a given location. Lastly, the combined station height dataset of 78.8–158.8 m with the Conv2D autoencoder reported the generalized score errors (ME = 0.105 m/s and RMSE = 0.420 m/s; ME = -3.10 and RMSE = 6.20) while the GRU score errors (ME = 0.019 m/s and RMSE = 0.396 m/s; ME = -2.90 and RMSE = 7.90) for the predictions without the feature noise removal are reported. © 2023 Journal of Energy Management and Technology

keywords: Offshore wind profiles, wind speed and direction variations, wind roses, frequency distributions, autoencoders, lidar measurements

http://dx.doi.org/10.22109/JEMT.2023.368508.1414

NOMENCLATURE

NWP Numerical Weather Prediction

MASCOT Microclimatic Analysis System for Complex Lands

WAsP Wind Atlas Analysis and Application Program

CNR Carrier to Noise Ratio averaged

FEEMD Fast Ensemble Empirical Model Decomposition

EEMD Ensemble Empirical Model Decomposition

LSSVM Least Squares Support Vector Machine

EFG Enhanced Forget Gate network

OST1–OST4 Offshore Station Heights (1–4) from Lidar System

ST1–ST4 Onshore Station Heights of Meteorological Masts

Conv2D 2–D Convolutional Neural Network (CNN)

Val Validation dataset

Val-loss Validation loss

WndDir Wind Direction

Air-Temp Air Temperature

MAE Mean Absolute Error

ML Machine Learning

SCADA Supervisory Control and Data Acquisition System

CFD Computational Fluid Dynamics

MOS Model Output Statistics

LAT Lowest Atronomical Tide

ITSM Improved Time Series Method

ESN Echo State Network

FNN Feedforward Neural Network

RNN RecurrentNeural Network

SVM Support Vector Machine

D Dimensional

AGL Above Ground Level

GRU Gated Recurrent Unit

Pred. Prediction dataset

Min Minimum

WndSpd Wind Speed

CoD Coefficient of Determination

RMSE Root Mean Square Error

WFTs Wind Forecast Tools

ELM Extreme Learning Machine

1. INTRODUCTION

In recent years, the capacity of the utility-scale wind system integration into the the electricity network has increased significantly and has become the main source of the renewable energy generation at a steady wind region. Due to the stochastic (intermittent) nature of the renewable resources (solar, wind and ocean waves) caused by climate effects, the utility-scale penetrations of wind turbine output into the interconnected grid-systems without the reliable forecast models have presented some operational challenges [1–4]. Also, apart from the challenges of maintaining the grid-system stability caused by energy resource intermittency, the negative impacts of climate effects have been recorded in other fields (agriculture, health and environment) [5, 6]. Based on the climate impacts resulting into: -1an energy resource flunctuation, 2sea level rising, 3soil erosion, 4high variations in the air temperature as well as 5the depletion of the ecosystems, the reliability of the machine learning (ML) in solving the time-series forecast problems of the air temperature and solar variations has been assessed at different locations. Based on the comparisons of different ML skills in the literature [7–13], the studied findings revealed that the ML model has emerged as an essential prediction tool in the: natural hazards assessment [7], solar system development and air-conditioning [8–10], short-term load predictions for the power utilities [11], cooling and energy consumption forecasting in the residential buildings [12, 13], adaptive temperature control of the greenhouse gases [14], assessment of the impact of the climate effects
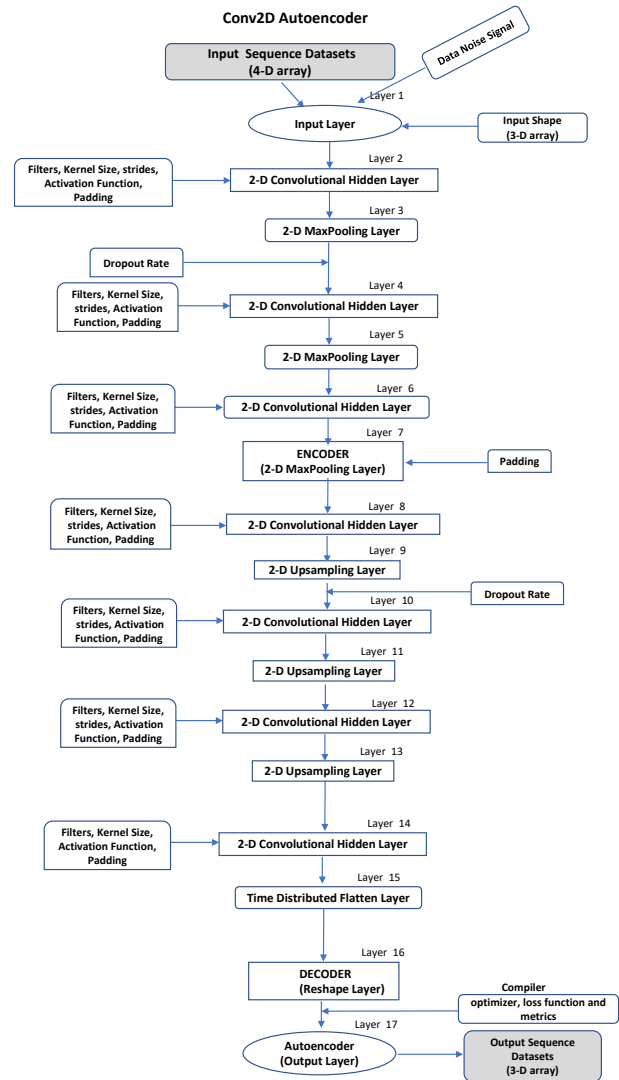

Fig. 1. Fig 1a: Block Diagram of a Conv2D Autoencoder (Unsupervised Predictive System)

on the photosynthetically active radiation [15], among others. In maintaining the reliability of the grid-connected wind energy systems, there has been a steady literature works in finding a reliable forecast model architecture(s) that could utilizes the combination of different spatial-temporal input feature datasets (such as: - topographic, relative humidity, air temperature, solar radiation, wind speed and direction, and atmospheric pressure) of a climatic region in portraying the historical and future wind power availability of a geographical multi-location [16–18]. For an optimal scheduling of the wind farm outputs into the transmission grid-network, the development of accurate forecasting model has been reported in the literature to be a crucial power tool in: 1planning operation of the electricity market pricing [19–21], 2electricity sustainability [22–24] and 3determining the reliability of the connected grid-systems [25–29]. The correlations and variations of the time-series of the offshore and onshore wind speed profiles, and turbine energy outputs at different climatic zones have been assessed in some literatures [30, 31]. Based on the temporal and spatial resolu-
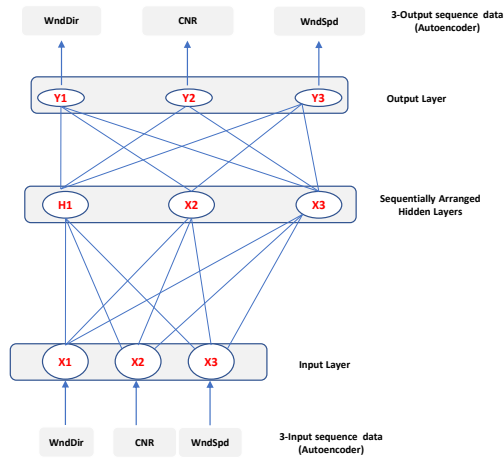
Fig 1b1: Schematic Diagram of an Autoencoder (Unsupervised Predictive System) for offshore station
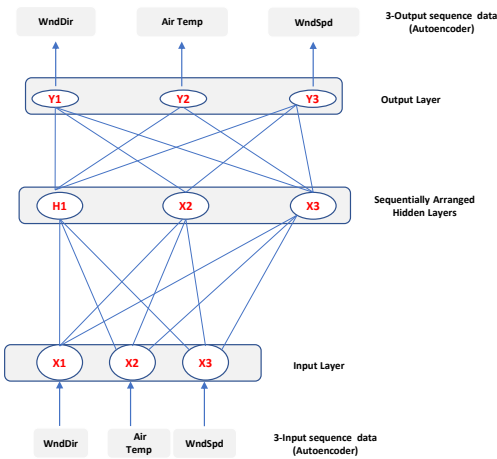

Fig. 2. Fig 1b2: Schematic Diagram of an Autoencoder (Unsupervised Predictive System) for onshore station

tions of the historical multivariate or/and univariate datasets obtained from different locations and data sources (SCADA, meteorological masts, numerical simulations, wind farm outputs, among others), a number of different wind forecast tools (WFTs) within the context of the time-series estimation of the wind speed or/and power outputs on the different time horizons (very-short, short, medium and long-term) [32] have been proposed but have deferred in model forecast skills. Also, to provide a more reliable estimates of the present or/and future wind power availability over the given time and space, several works have been made in reducing the uncertainty (model errors) of the time-series forecasts by developing a single or combination of different WFTs with various resolution input datasets such as:- 1Physical Models (NWP with Kalman filter [33], MASCOT [34, 35], CFD modeling [36], Prediktor "HIRLAM forecast with the WAsP and MOS models [37]", Previento [38]); 2Statistical Models (VAR [39], ARIMA with ARCH [40], wavelet transfor-

mation with ITSM [41], univariate ARIMA and multivariate NARX [42]); 3Machine Learning (ML) (ESN, FNN and the fuzzy inference system [43]; FEEMD with LSSVM [44], EEMD with the LSSVM [45], Wavelet RNN [46], ESN [47, 48], LSTM [49], LSTM with the ESN [1], Spiking NN [50], ARIMA with Radial Basis NN [51], EEMD with LSTM and EFG [51], CNN with GRU and ANN [29], SVM [52], LSTM encoding-decoding network model [53]); among others. Within the context of the onshore
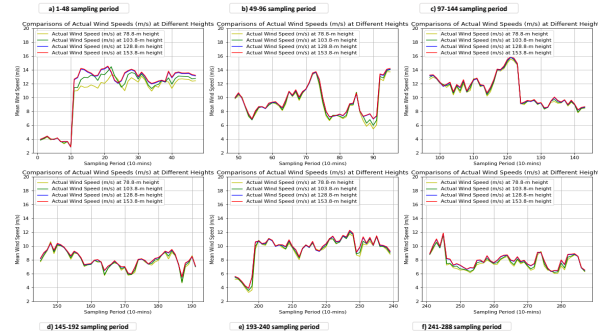

Fig. 3. Fig 2: Time-series of actual offshore wind speed profiles (m/s) at different measured heights (OST1 - OST4)

and offshore wind speed and power forecasting, a huge success and breakthrough (superiority) of the ML over the Physical and Statistical Models has been recorded in most recent times [54–57]. Also, the spatial-temporal correlation ability (features input extraction and model generalization) of the ML has been investigated in time-series forecast problems [58, 59] and has proven to be more accurate in model forecast skill than the physical and statistical models. In the time-series wind forecast problems using the various multivariate datasets, Chen et al [55] have utilized the LSTM-CNN for the energy forecast solutions of multiple wind turbine systems at a wind farm location; Shabbir et al [60] have utilized the RNN-LSTM in the wind energy forecasting of Estonia; Huang et al [61] proposed the genetic algorithm (GA) and LSTM model in a wind speed forecasting; Cali and Sharma [62] have utilized the RNN-LSTM for short-term wind power forecasting; Anushalini and Revathi [63] have investigated the suitability of the LSTM model in the time-series wind power forecasts; Fu et al [64] have considered an improved chicken swarm algorithm optimization support vector machine (ICSO-SVM) for the wind power predictions. Based on an improved LSTM, Wang et al [65] proposed the wind power forecasting model; Zhang et al [66] have proposed an hybrid decomposition and robust ELM in time-series wind speed predictions. Further to this; Kumar and Ali [67], Sharifzadeh et al [7], Sun et al [68] and Demolli et al [69] have considered and compared a different ML technique for the wind power forecasts based on the different temporal datasets.

Although, the 1number and layout of the network layers in a designed forecast model architecture, 2selected learning algorithm(s) as well as the 3batch size of an input features dataset are important parameters that positively infuence how the multivariate non-linear input features are processed/trained in the model architecture, however, the two main limitations of the WFTs in the time-series wind forecasting are as follow: 1poor model performance (high deviation) for multivariate non-linear input datasets scheduled on long-term forecast horizon and the 2network complexity (high computational cost and time) as a

result of an increasing network layers. To solve (address) but the time-series (long-term) forecast problem associated with the model high deviation for a multivariate non-linear input feature dataset, our wind study proposes two autoencoding architectures that entail the combination of a 2–stage process for handling the uncertainty of the multivariable non-linear forecasts. In finding the baseline forecast architecture for: - 1describing the variability (non-linear forecast solutions) and 2analysing the time-series of the offshore and onshore wind profiles of a specific climatic region, 2-different autoencoding architectures (Conv2D and GRU encoding-decoding networks) in an unsupervised operation are investigated and compared. Our proposed forecast models have robust capability to adopt to self-learning from the non-linear input features of the multivariables station datasets. Sequel to this, our two autoencoding architectures are sequentially arranged such that it accept a 3–variable input sequence and also produce the hourly forecast of a 3–variable non-linear output sequence for the considered onshore and offshore station heights. Also, the feature noise technique is introduced allowing for better improvement/modeling and forecasting processes of the historical input data sequence(s). Hence, the objective of this study is aimed at developing and evaluating the forecast accuracy skills of 2–different autoencoding architectures that could be utilized for the time-series prediction (unsupervised ML) and the analysis of the offshore, as well as in onshore station mutlivariable profiles at different geographical zones. For this present
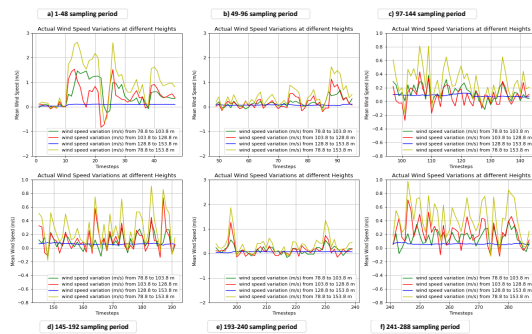

Fig. 4. Fig 3: Time-series of actual offshore wind speed variations (m/s) at different measured heights (OST1 - OST4)

study, the time-series forecasts and analysis of the offshore and onshore station multivariables (1wind speed, 2direction, 3air-temperature and 4CNR) of the lidar and meterological measurement systems at 8–heights are carried out at a sampling period of 48–timesteps. The historical multivariable datasets of 5–min and 10–min intervals at two geographical zones are collected while the input-feature noise correction is introduced/incorporated into our proposed architectures for an enhanced model forecast skill(s). Two autoencoding model architectures (Conv2D and GRU encoding-decoding layers network) in an unsupervised predictive operation are built in Tensorflow2.0 (Figures 1 and S1). The sequentially arranged network layers of the Conv2D autoencoder are built with a 4–D input data structure while the sequentially arranged network layers of the GRU autoencoder are designed with a 3–D input data structure. At the sampling of 48 timesteps, the Conv2D and GRU autoencoders in the time-series predictions and analysis of a 3–D input variables sequence (WndDir, WndSpd and CNR for the offshore station heights; WndDir, WndSpd and Air Temperature for the onshore

heights) are proposed. Furthermore, our investigated autoencoders are evaluated with an independent dataset collected from the remote 5–energy buildings. At different heights, our studied findings of the wind profiles are compared in determining the: 1WndDir and WndSpd variation heights, and 2steadiest wind height ideal for an optimum energy resource conversion. The dominant wind flow (rose) driven by the atmospheric or/and the local surface irregularities at the station heights (10–20 m) are assessed as well. Lastly, the frequency distributions of the offshore and onshore wind profiles with and without the feature noise eliminations are compared. It is believed that this energy study would provides a platform for investigating and demonstrating the importance of the GRU and Conv2D autoencoders in time-series multivariable predictions and analysis at different geographical zones and heights.
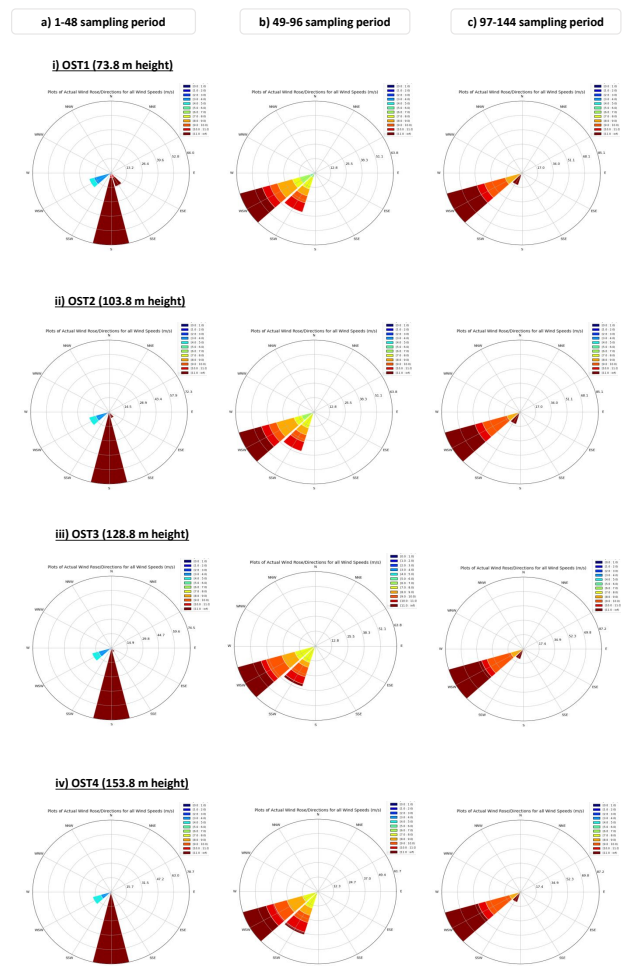

Fig. 5. Fig 4: Actual model comparisons of offshore wind roses at different measured heights (OST1 - OST4)

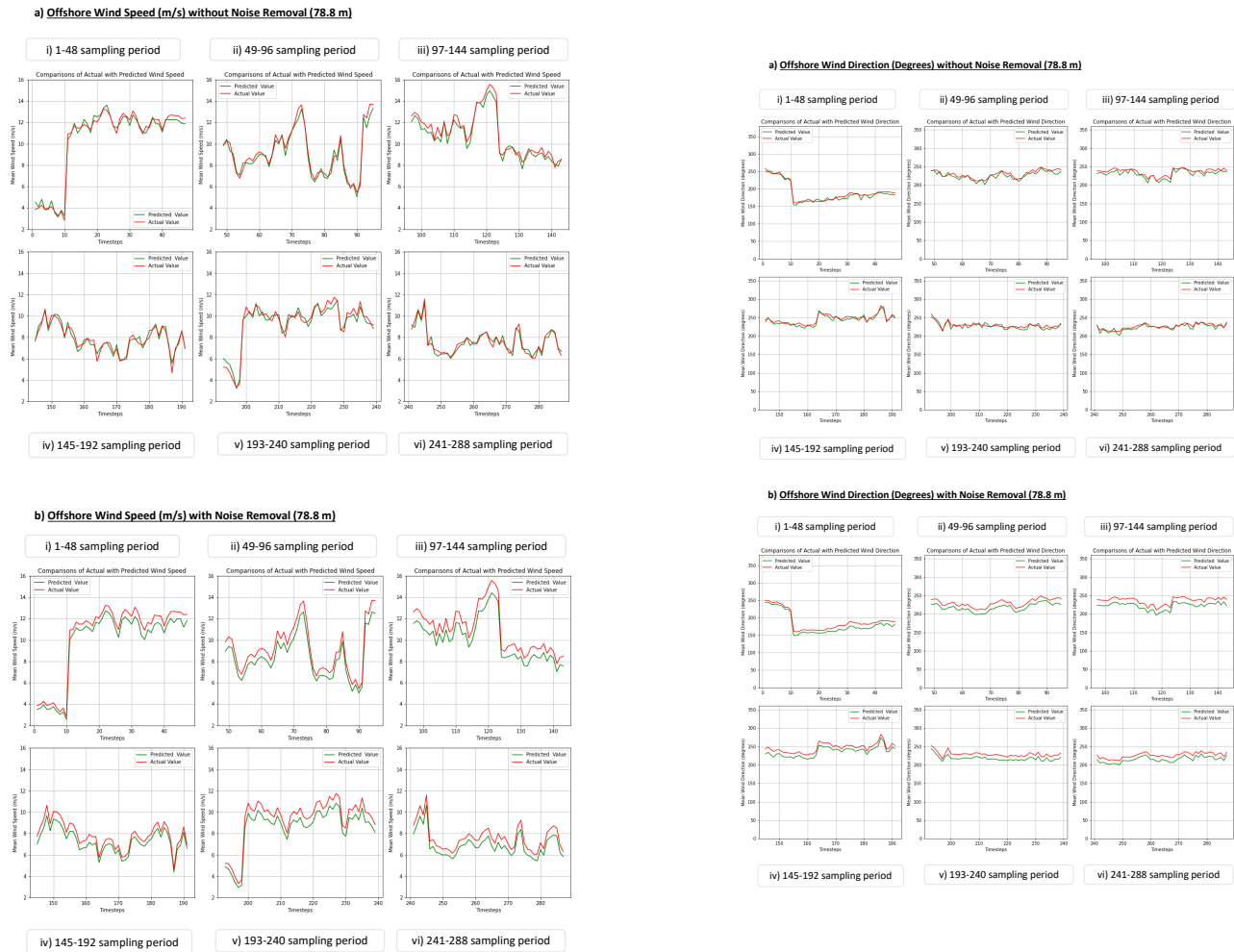Table 2) are obtained. The time-series multivariable datasets of

Fig. 6. Fig 5: Actual and Conv2D autoencoder plots of offshore wind speed (m/s) without and with noise removal at OST1

Fig. 7. Fig 6: Actual and Conv2D autoencoder plots of offshore wind direction (degrees) without and with noise removal at OST1

2. DATASET COLLECTION AND DESCRIPTION

The data collection and description of the experimental offshore and onshore stations at sampling time of 5–min/10–min (Col. 2 of Table 1a) and period (Cols. 3–4) are summarized in Table 1. The selected historical datasets of the station variables from the: 1lidar measurements of the offshore heights (OST1–OST4) and 2meteorological masts (ST1–ST4) of the onshore measurements are summarized in the Col 6. The lidar measurement systems are installed on Westermost Rough WindFarms (North Sea of England) for the offshore wind data measurements at GPS station (see Col. 5). The lense height of the lidar system is referenced to a LAT positioning of 33.8 m height of which the offshore measurements are obtained and adjusted to the new heights (73.8, 103.8, 128.8 and 153.8 m). Meanwhile, the meteorological sensors for the onshore stations in the Western Cape of South Africa are installed on the masts AGL for which the data measurements at different onshore station heights (Col. 2 of

each GPS station height (Col. 6) are obtained in 2–D data structure and used for the: 1autoencoder development, and 2analysis of the offshore and onshore wind profiles at each station height. For each offshore height (OST1/OST3/OST4), the total data samples per station variable are reported in Col 7 of Table 1a and pre-processed as the: 1training (Col. 8) and 2prediction (Col 9) input data sequence (that is, 91.1 and 8.89 % of the total data samples, respectively). For each onshore station height (ST1/ST3/ST4), 94.6 and 5.40 % of the total sample datasets are also preprocessed as: 1training and 2prediction input sequence datasets, respectively. Meanwhile, for the autoencoder validation process, 91.1 and 100 % of the new samples are obtained from the additional offshore (OST2) and onshore (ST2) station heights, respectively. For the autoencoder model skills evaluation, these are measured with independent evaluation data (Res-Ev1–Res-Ev5) on an hourly basis (Cols 3–4 of Table 1c). A detailed information of the offshore station datasets as well as the evaluation datasets of the selected station variables is documented in the reports [70, 71]. The time-series of the actual offshore wind speeds (m/s) and directions(degrees) for the total
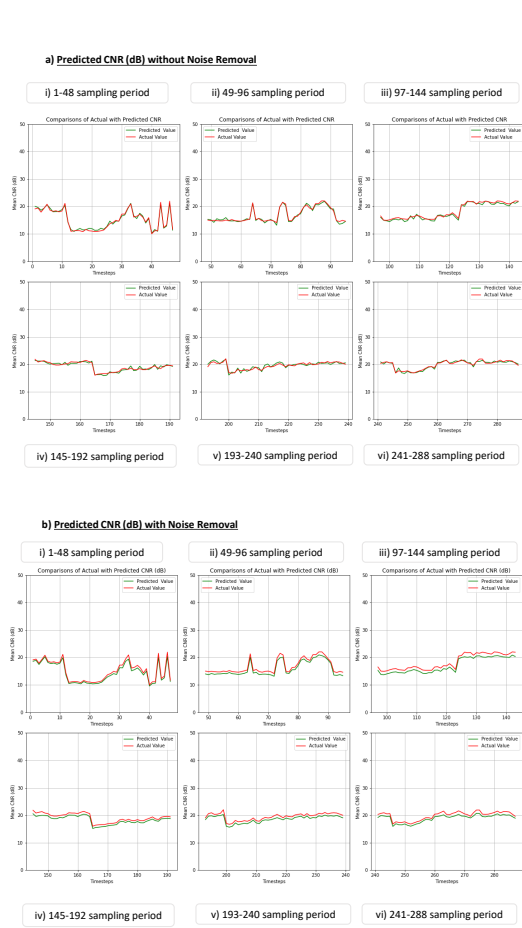
Fig. 8. Fig 7: Actual and Conv2D autoencoder plots of offshore CNR (dB) without and with noise removal at OST1

Fig. 9. Fig 8: Actual, Conv2D and GRU autoencoder comparisons of offshore wind roses at different measured heights (1-288 steps)

sampling period of 1–288 steps at different measurement heights (OST1 –OST4) are provided in Figs 2 and S2, respectively. For the regular sampling period of 48 timesteps, the actual wind roses (12-sectorwise wind flow) for the offshore station heights (OST1–OST4) are summarized (Table 2, Figs. 4 and S4) while the Fig. S5 summarizes the actual wind roses of the onshore stations (ST1–ST4). From the figurative comparisons (time-series of the offshore 1wind speed and direction, and 2sectorwise wind rose for the height of 78.8 – 153.8 m), our findings (Figs. 3 and S3) show that the offshore wind profiles of the lidar measurements are subjected to the prevailing synoptic conditions of 78.8 – 128.8 m height but becomes steadier and ideal at above 128.8–153.8 m height for optimal loading of the offshore wind energy turbines. However, the onshore wind profiles of the stations (ST1–ST4) show that the actual directions of wind flow (Fig. S5) are mainly driven by the local effects and prevailing synoptic conditions, with exception to ST4 with unidirectional wind flow. The sample size of the time-series datasets of 3–variable per station height (Cols 7–9 of Tables 1a) is reproduced from its original size of 2–D input data structure (Col 2 of Table 1b) to a: 1new input data array "4–D" for the Conv2D autoencoder (Cols 3–5 of Table 1b); 2new input data array "3–D" for the GRU autoencoder (Cols 6–8
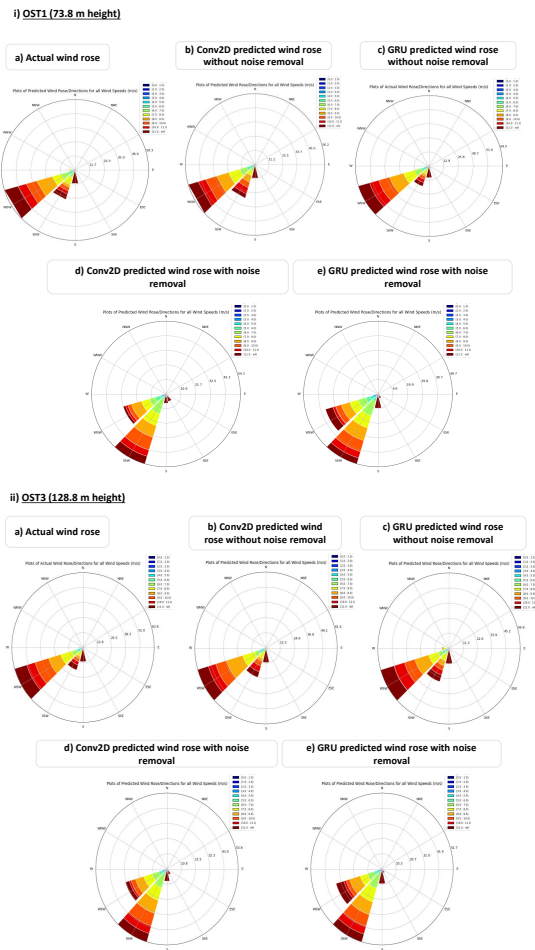
of Table 1b). The input data configurations of the Conv2D and GRU autoencoders are summarized in Cols. 3–8 of Table 1b.

3. METHODOLOGY

The workflow of the investigated autoencoding model architectures in an unsupervised predictive operation are built in Tensorflow2.0 as depicted in Figs. 1 and S1. The sequentially arranged layers of the Conv2D autoencoder (Fig. 1) was designed with the 4–D input data array and 3–D output sequence structures ('WndSpd, WndDir and CNR' for the offshore heights; 'WndSpd, WndDir and Air_Temp' for the onshore station). Also, the sequentially arranged layers of the GRU autoencoder (Fig. S1) was designed with a 3–D input data array and a 3–D output data sequence structures. The block diagrams of the study models of Fig. 1 (Conv2D autoencoder) and Figs S1 (GRU autoencoder) are described in the section 3.3.1 and 3.3.2. In learning the dynamics of the non-linear input data sequence (input features), the network optimizer of the Adamax version of the stochastic gradient descent (training algorithms) for our autoencoding processes was utilized, while the tanh function for the activation of the input and hidden layers of each autoencoding process was
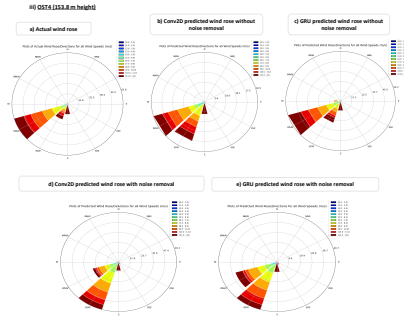
Fig. 10. Fig 8: Actual, Conv2D and GRU autoencoder comparisons of offshore wind roses at different measured heights (1-288 steps)

utilized. Finally, the Conv2D and GRU autoencoding models generate the time–series multivariable predictions for the 3–D input sequence variables at the data sampling horizons of every 48–timesteps.

A. Lidar Wind Data Correction

For an accurate assessment of the offshore wind profiles from the lidar measurement systems, data corrections were introduced. The lidar lense height was considered and referenced to a LAT positioning of 33.8 m height of which the measurement datasets were taken and adjusted to the actual measurement heights of 73.8, 103.8, 128.8 and 153.8 m ASL above LAT. That is, the lidar data correction was carried out with the offset wind direction value in determining the actual: 1. wind direction and 2. measurement height above the LAT as follow:

a)the actual wind direction for a new measurement height (H) above LAT position was calculated from the lidar wind direction of the measuring height with an offset wind direction value:

$$Actual\ wind\ direction(0) =$$
$$lidar\ measured\ wind\ direction\ - offset\ wind\ direction\ value$$
$$\text{(1)}$$

b) the actual measurement height for an offshore station is calculated by considering the configured measuring height with the lidar lense height above LAT position (h = 33.8 m):

$$Actual measurement height\ (m)\ =$$
$$configured measuring height + lidar height of the lense\ (h)$$
$$\text{(2)}$$

$$A_{io} = \frac{(A_{(inp,i)} - A_{(inp,\min)})}{(A_{(inp,\max)} - A_{(inp,\min)})} \qquad \text{(3)}$$

where $A_{(inp,i)}$ is the actual measured datasets for the station (> 0) at a given instance i;$A_{(inp,min)}$ and $A_{(inp,max)}$ are the
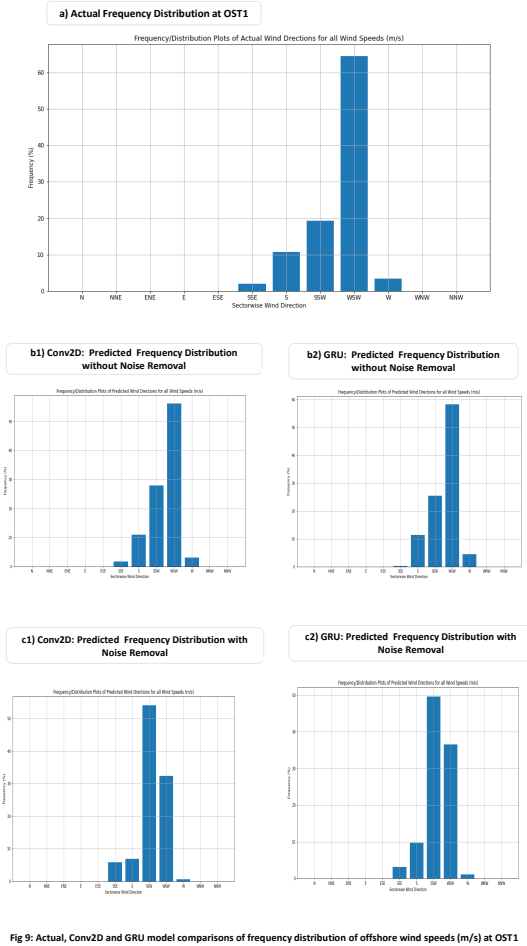
Fig 9: Actual, Conv2D and GRU model comparisons of frequency distribution of offshore wind speeds (m/s) at OST1

Fig. 11. Fig 9: Actual, Conv2D and GRU model comparisons of frequency distribution of offshore wind speeds (m/s) at OST1

minimum and maximum values of the input variable dataset (feature), respectively;A_{io} is the normalized dataset.

Next, the normalized/scaled-down input dataset of Eq. 3 was reshaped according to the autoencoder specification of accepting input sequence data into a 1st network layer. Using the reshaping argumentation below, the 2–D normalized input dataset was re-structured/re-calculated into a: 14–D input sequence dataset (A_{io}_Conv2D) for the Conv2D layer architecture (Fig 1), 23–D input sequence dataset (A_{io}_GRU) for the GRU autoencoder (Fig. S1):

$$A_{io}\_Conv2D =$$
$$A_{io}.reshape\ (timesteps, input\_features, samples, batch\_size)$$
$$\text{(4)}$$

$$A_{io}\_GRU =$$
$$A_{io}.reshape\ (timesteps, input\_features, samples)$$
$$\text{(5)}$$

where the timesteps = 10332 and 1008 for the autoencoder input training/prediction of the offshore, respectively; timesteps =

Table 1. Table 1a: Data description of the experimental offshore and onshore stations.

Offshore	Sampled Time	Sampled Period DD-MM-YYYY	Station GPS HH:MM:SS	Station GPS (LIDAR)	Station Variables m/s, degree, dB	Sample per Variable	Training Sample per Variable	Prediction Sample per Variable
OST1	10-mins	22-Aug 2014 - 19-Apr 2018	00:00:00- 00:50:00	56.440677N/ 8.150692E	WndSpd, WndDir, CNR	11340	10332	1008
OST3	10-mins	22-Aug 2014 - 19-Apr 2018	00:00:00- 00:50:00	56.440677N/ 8.150692E	WndSpd, WndDir, CNR	11340	10332	1008
OST4	10-mins	22-Aug 2014 - 19-Apr 2018	00:00:00- 00:50:00	56.440677N/ 8.150692E	WndSpd, WndDir, CNR	11340	10332	1008
Validation	Time							
OST2	10-mins	22-Aug 2014 - 19-Apr 2018	00:00:00- 00:50:00	56.440677N/ 8.150692E	WndSpd, WndDir, CNR	11340	10332	——
Onshore	Sampled Time	Sampled Period DD-MM-YYYY	Station GPS HH:MM:SS	Station GPS Meteorological	Station Variables m/s, degree, oC	Sample per Variable	Training Sample per Variable	Prediction Sample per Variable
ST1	10-mins	01-Jul 2011 - 02-Jan 2011	00:10:00 - 24:00:00	WM03	WndDir_20, WndSpd_20, Air_Temp	26640	25200	1440
ST3	10-mins	01-Jul 2011 - 02-Jan 2011	00:10:00 - 24:00:00	WM02	WndDir_20, WndSpd_10, Air_Temp	26640	25200	1440
ST4	5-mins	15-Aug 2010 - 06-Jan 2011	18:10:00 - 00:25:00	PWS	WndDir_10, WndSpd_10, Air_Temp	26640	25200	1440
Validation	Time							
ST2	5-mins	01-Jan 2006 - 13-Dec 2006	00:05:00 - 11:55:00	GWS	WndDir_10, WndSpd_10, Air_Temp	21600	21600	——

Table 2. Table 1b: Description of data input configurations (model training, validation and prediction) for the autoencoders.

Offshore Training/Prediction	Total Sampling Datasets	Data Configuration Conv2D	Model Training Data Conv2D	Model Prediction Data Conv2D	Data Configuration GRU	Model Training Data GRU	Model Prediction Data GRU
OST1	(11340x3)	(11340x3x1x1)	(10332x3x1x1)	(1008x3x1x1)	(11340x3x1)	(10332x3x1)	(1008x3x1)
OST3	(11340x3)	(11340x3x1x1)	(10332x3x1x1)	(1008x3x1x1)	(11340x3x1)	(10332x3x1)	(1008x3x1)
OST4	(11340x3)	(11340x3x1x1)	(10332x3x1x1)	(1008x3x1x1)	(11340x3x1)	(10332x3x1)	(1008x3x1)
Validation	Total Sampling	Data Configuration	Model Validation	Model Prediction Data	Data Configuration	Model Validation	Model Prediction Data
OST2	(11340x3)	(11340x3x1x1)	(10332x3x1x1)	———	(11340x3x1)	(10332x3x1)	———
Onshore	———	—————	—————	————	—————	————	———
Training/Prediction	Total Sampling	Data Configuration	Model Training Data	Model Prediction Data	Data Configuration	Model Training Data	Model Prediction Data
ST1	(26640x3)	(26640x3x1x1)	(25200x3x1x1)	(1440x3x1x1)	(26640x3x1)	(25200x3x1)	(1440x3x1)
ST3	(26640x3)	(26640x3x1x1)	(25200x3x1x1)	(1440x3x1x1)	(26640x3x1)	(25200x3x1)	(1440x3x1)
ST4	(26640x3)	(26640x3x1x1)	(25200x3x1x1)	(1440x3x1x1)	(26640x3x1)	(25200x3x1)	(1440x3x1)
Validation	Total Sampling	Data Configuration	Model Validation	Model Prediction Data	Data Configuration	Model Validation	Model Prediction Data
ST2	(21600x3)	(21600x3x1x1)	(21600x3x1x1)	———	(21600x3x1)	(21600x3x1x1)	———

Table 3. Table 1c: Description of input data configurations for the autoencoder evaluations.

| Buildings Evaluation	Total Sampling Datasets	Residential Variables (kWh)	Model Evaluation Data Conv2D	Model Evaluation Data GRU
Res-Ev1	(8760x3)	Fans, Cooling and Electricity Supply	(8760x3x1x1)	(8760x3x1)
Res-Ev2	(8760x3)	Fans, Cooling and Electricity Supply	(8760x3x1x1)	(8760x3x1)
Res-Ev3	(8760x3)	Fans, Cooling and Electricity Supply	(8760x3x1x1)	(8760x3x1)
Res-Ev4	(8760x3)	Fans, Cooling and Electricity Supply	(8760x3x1x1)	(8760x3x1)
Res-Ev5	(8760x3)	Fans, Cooling and Electricity Supply	(8760x3x1x1)	(8760x3x1)
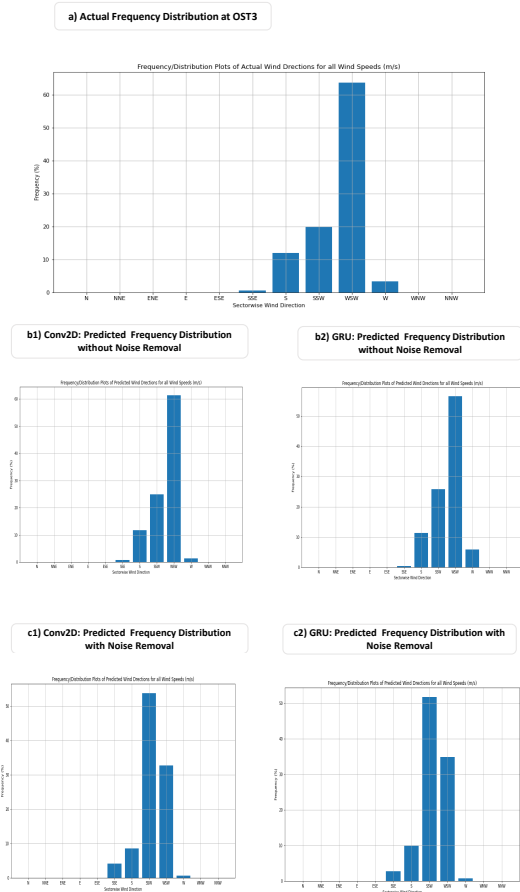
Fig. 12. Fig 10: Actual, Conv2D and GRU model comparisons of frequency distribution of offshore wind speeds (m/s) at OST3

Fig. 13. Fig 11: Conv2D plots of onshore a-bwind speed (m/s) and c-ddirection (degrees) without and with noise removal at ST1

25200 and 1440 for the autoencoder training and prediction of each onshore height, respectively; input features = 3 for the offshore and onshore station variables (Cols. 4-8 of Table 1b); samples = 1 and batch_size = 1 Note: The total sampling dataset of each offshore station height was divided into: 1batch_data1 represented as the normalized input training dataset of the autoencoder and 2batch_data2 represented as the normalized input prediction dataset of the model. Batch_data1 [A_{io} (t1)–A_{io} (t10332)] has an input data configuration of '[10332x3x1x1] for Conv2D model and [10332x3x1] for the GRU' while the batch_data2 [AA_{io} (t1)–AA_{io} (t1008)] has an input data configuration of '[1008x3x1x1] for a Conv2D autoencoder and [1008x3x1] for the GRU model'. Meanwhile, the normalized input data for the onshore stations was also divided into: batch_data1 [A_{io} (t1)–A_{io} (t25200)] with an input data configuration of '[25200x3x1x1] for the Conv2D and [25200x3x1] for the GRU autoencoder' while the batch_data2 [AA_{io} (t1) – AA_{io} (t1440)] has an input data configuration of '[1440x3x1x1] for the Conv2D autoencoder and [1440x3x1] for the GRU autoencoder'. For the autoencoder prediction datasets (batch_data2) of the: - 1offshore [AA_{io} (t1)–AA_{io} (t1008)] for the sampling period of 1008 timesteps and 2onshore
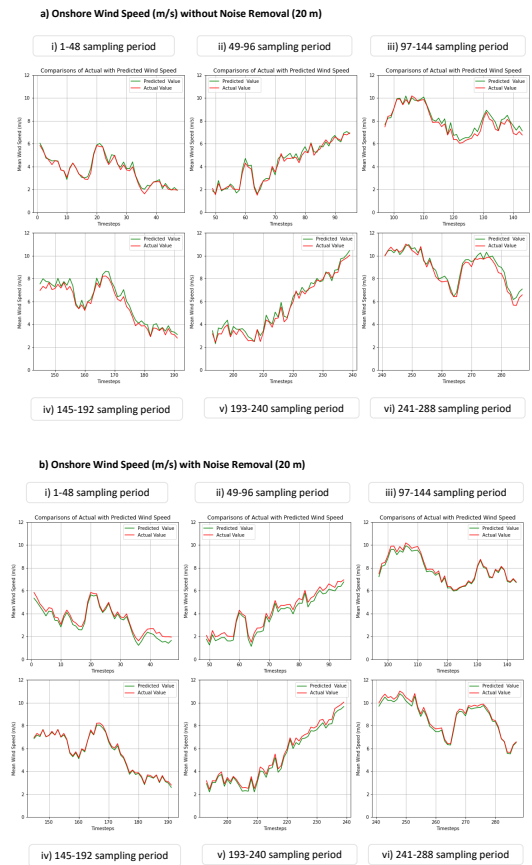
['AA_{io} (t1)–AA_{io} (t1440)] for the period of 1440 timesteps, the expected model outputs (3-variable) of the autoencoder for each station height generates the time-series forecasts in model output sizes of [1008x3x1] for the offshore stations and [1440x3x1] for an onshore station. The summary of the input data configurations for the investigated Conv2D and GRU autoencoders was depicted in Table 1b. Thereafter, we introduced the feature noise signal into the input data sequence of Eqs. (4)–(5) for better performance of the investigated autoencoding model. The mathematical expressions for obtaining the input noisy data sequence were as follow:

$$y\_random = numpy.random.rand(A_{io}.shape[0], 1) \quad (6)$$

$$feature\ noise\ signal = (noise\_factor * y\_random) \quad (7)$$

$$A_{io}\_Conv2D\_noisy = \\ np.clip((A_{io}\_Conv2D + feature\ noise\ signal), 0, 1) \quad (8)$$

Table 4. Table 2: Summary of the dominant sectorwise wind directions for the actual wind flows at different station heights.

| Offshore	Station Heights (m)	Sampling 1-48 steps	Sampling 49-96 steps	Sampling 97-144 steps	Sampling 145-192 steps	Sampling 193-240 steps	Sampling 241-288 steps
OST1	73.8	S	WSW & SSW	WSW	WSW	WSW	WSW & SSW
OST2	103.8	S	WSW & SSW	WSW	WSW	WSW	WSW & SSW
OST3	123.8	S	WSW & SSW	WSW	WSW	WSW	WSW & SSW
OST4	153.8	S	WSW & SSW	WSW	WSW	WSW	WSW & SSW
Onshore	Heights (m)	1-48 steps	49-96 steps	97-144 steps	145-192 steps	193-240 steps	241-288 steps
ST1	20	S & SSE	SSE	W, WSW & WWN	WSW	S	W & WSW
ST2	10	SSE	ESE	SSW, S, WSW	WNW & W	WNW	W
ST3	20	SSE & ESE	ESE	WSW, SSW, W	WSW & S	S	S
ST4	10	ENE	ENE	ENE	ENE	ENE	ENE
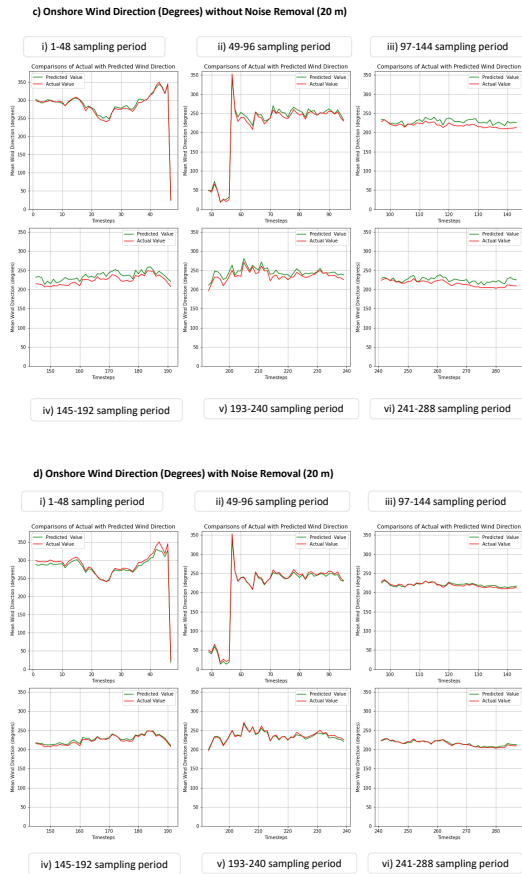
Fig. 14. Fig 11: Conv2D plots of onshore a-bwind speed (m/s) and c-ddirection (degrees) without and with noise removal at ST1

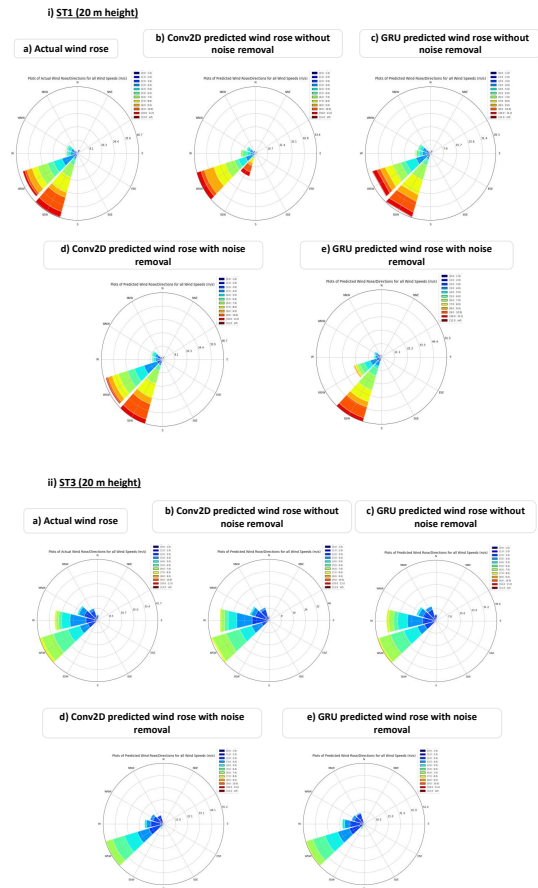**Fig. 15.** Fig 12: Actual, Conv2D and GRU autoencoder comparisons of onshore wind roses at ST1 and ST3, respectively (1-288 steps)

$$A_{io}\_GRU\_noisy =$$
$$np.clip((A_{io}\_GRU + feature\ noise\ signal), 0, 1) \quad \textbf{(9)}$$

where the noise_factor =0.05; $A_{io}\_Conv2D\_noisy$ and $A_{io}\_GRU\_noisy$ represent the input sequence dataset with the noise signal inclusion for the Conv2D and GRU autoencoders, respectively. The procedures in Section 3.3.1–3.3.2 and Appendix 1–2 were utilized for the predictions of the time-series of the offshore/onshore station input 3–variables. Once the long-term predictions of the station height variables (WndSpd, WndDir, CNR and Air-Temp) for the investigated timesteps have been generated, the de-normalization operation was carried out on the predicted values. For the forecast values without the removal of the feature noise signal, these were obtained as:

$$\bar{A}_{Conv2D(inp.i)} = \bar{A}_{io}(A_{(inp,\max)} - A_{(inp,\min)}) + A_{(inp,\min)} \quad \textbf{(10)}$$

$$\bar{A}_{GRU(inp.i)} = \bar{A}_{io}(A_{(inp,\max)} - A_{(inp,\min)}) + A_{(inp,\min)} \quad \textbf{(11)}$$

where $A\_Conv2D(inp.i), A\_GRU(inp.i)$ and $\bar{A}\_io$ denote the de-normalized forecast value of Conv2D and GRU autoencoder

without the feature noise removal, time-series predictions of the Conv2D or GRU autoencoder for each station height, respectively. For the predicted values with the removal of noise signal, the de-normalization operation was carried out as follows:

$$\bar{A}_{oConv2D(inp,i)} = \bar{A}_{Conv2D(inp.i)} - (feature\ noise\ signal) \quad \textbf{(12)}$$

$$\bar{A}_{oGRU(inp,i)} = \bar{A}_{GRU(inp.i)} - (feature\ noise\ signal) \quad \textbf{(13)}$$

where $\bar{A}_{oConv2D(inp,i)}$ and $\bar{A}_{oGRU(inp,i)}$ denote the de-normalized forecast values of the Conv2D and GRU with the feature noise signal removal, respectively.

A.1. Conv2D Autoencoding Architecture

The block diagram of the Conv2D autoencoding architecture in an unsupervised predictive operation was presented in Fig. 1. Our Conv2D autoencoder was built with a 17–sequentially arranged network layer. For this model setup, a 4–D normalized input dataset with the feature noise signal (Eq. 8) was

Table 5. Table 3a: System architecture of Conv2D autoencoder Model: "model_1"

| Layer (type)	Output Shape	Param #
input_1 (InputLayer)	(None x3x1x1)	0
conv2d_1(Conv2D)	(None x3x1x180)	1800
max_pooling2d_1 (MaxPooling2)	(None x3x1x180)	0
dropout_1 (Dropout)	(None x3x1x180)	0
conv2d_2(Conv2D)	(None x3x1x144)	233424
max_pooling2d_2 (MaxPooling2)	(None x1x1x144)	0
conv2d_3(Conv2D)	(None x3x1x108)	140076
max_pooling2d_3 (MaxPooling2)	(None x1x1x108)	0
conv2d_4 (Conv2D)	(None x1x1x108)	105084
up_sampling2d_1 (UpSampling2)	(None x3x1x108)	0
dropout_2 (Dropout)	(None x3x1x108)	0
conv2d_5 (Conv2D)	(None x3x1x144)	140112
up_sampling2d_2 (UpSampling2)	(None x3x1x144)	0
conv2d_6 (Conv2D)	(None x3x1x180)	233460
up_sampling2d_3 (UpSampling2)	(None x3x1x180)	0
Con2d_7 (Conv2D)	(None x3x1x1)	4501
time_distributed_1 (TimeDist)	(None x3x1)	0
reshape_1 (Reshape)	(None x3x1)	0
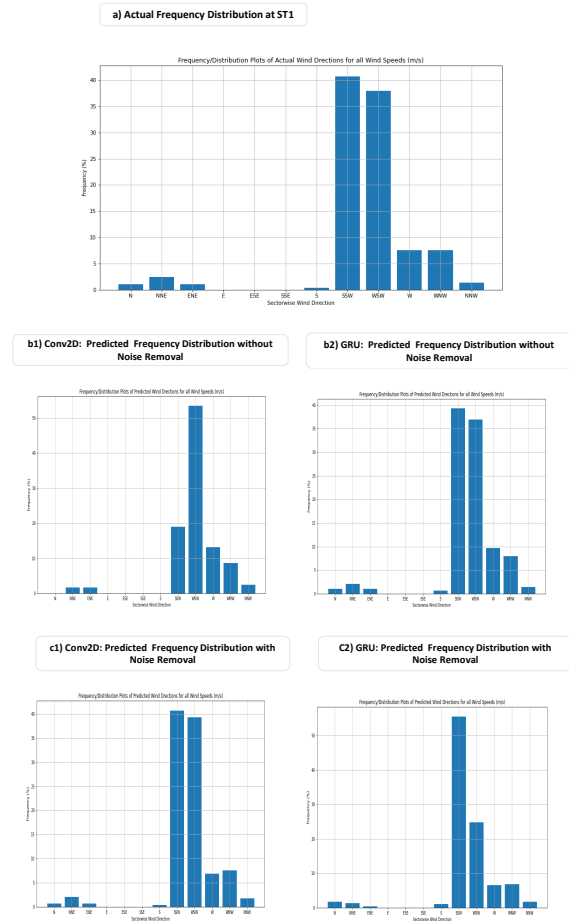
Fig. 16. Fig 13: Actual, Conv2D and GRU model comparisons of frequency distribution of onshore wind speeds (m/s) at ST1

used as the autoencoder input data sequence while the hyperparameters that influence the model learning and prediction ability from the input to output network layers were identified, and initialized before the network layers was compiled. For the autoencoding architecture of Fig. 1, the following model hyperparameters were selected: convolutional filters with 180, 144 and 108 neurons ('1st, 2nd and 3rd hidden layers', respectively) before the encoding process; additional 108, 144, 180 and 1 neurons (4th, 5th, 6th and 7th hidden layers, respectively) after the encoding process; kernel-size of 2–D convolutional window = (3,3) and (5,5); batch-size = 5; number of iterations (nb_epoch) = 30; kernel-initializer = glorot_uniform; number of output variables (nb_classes) = 3; dropout regularization rate = 35 % (ensuring unused or randomly selected neurons were ignored); strides value = (1,1); tanh function to activate the input and hidden layers but the sigmoid function for output layer activation. Other parameters used in the autoencoder build-up and training process were summarized in the Appendix 1. For the network compilation, our autoencoder was designed with the: 1network optimizer of Adamax version of stochastic gradient descent (learning algorithm), 2loss function (mean_square_error, MSE) and the 3model metric (mean_absolute_error, MAE) for
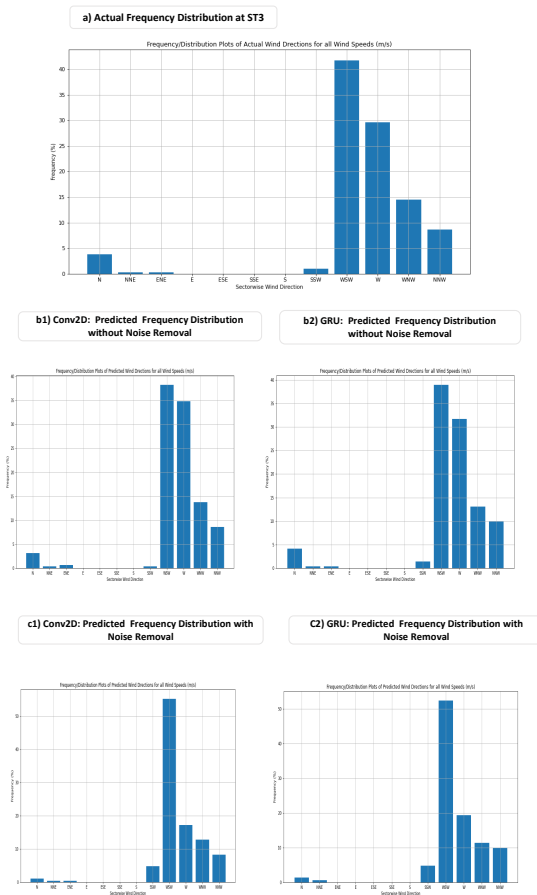
Fig. 17. Fig 14: Actual, Conv2D and GRU model comparisons of frequency distribution of onshore wind speeds (m/s) at ST3

Table 6. Table 3b: System architecture of GRU autoencoder Model: "sequential_1"

Layer (type)	Output Shape	Param #
input_10 (InputLayer)	(None x3x1)	0
gru_218(GRU)	(None x3x80)	98280
dropout_62 (Dropout)	(None x3x180)	0
gru_219(GRU)	(None x3x144)	140400
gru_220(GRU)	(None x3x108)	81972
batch_normalization _31(Batch)	(None x3x108)	70308
dropout_63 (Dropout)	(None x3x108)	0
gru_222(GRU)	(None x3x144)	109296
gru_223(GRU)	(None x3x180)	175500
gru_224(GRU)	(None x3)	1656
reshape_8 (Reshape)	(None x3x1)	0

dataset for the autoencoder while the hyperparameters that influence the model learning and prediction ability of the autoencoder from the input to output network layers were identified, and initialized before the network layers was compiled.

For the GRU autoencoder of Fig. S1, the following model hyperparameters were selected: gated mechanism filters with 180, 144 and 108 neurons ('1st, 2nd and 3rd hidden layers', respectively) before the encoding process; but additional 108, 144, 180 and 3 neurons (4th, 5th 6th and 7th hidden layers, respectively) after the encoding process; the return sequence of gated window=True; batch-size = 5; number of iterations = 30; kernel-initializer = glorot_uniform; number of output variables (nb_classes) = 3; dropout regularization rate = 35 %; tanh function to activate the input and hidden layers but the sigmoid function for an output layer activation. Other parameters used in the autoencoder build-up and training process were summarized in the appendix 2. For the network compilation, our autoencoder was designed with the similar: 1network optimizer, 2loss function and 3model metric of Section 3.3.2 for assessing the GRU autoencoder performance(s).

The spatial input features (normalized input sequence data) of the input layer were passed to the 1st connected hidden layer with the tanh activation function. From the 1st GRU hidden layer, the processed sequence samples were passed into the subsequent GRU hidden layers via a repeated mechanism until the last hidden layer (layer 9) further narrows the sequence array from the 3–D [1x3x180] into 2–D output shape [1x3]. Thereafter, the GRU hidden layer passed the 2–D sequence data array into the reshape layer (decoder). The reshape layer extracts the wrapped input sequence samples (2–D) from the last GRU hidden layer and reshaped them for the autoencoder predictions before passing through to the output layer nodes with a 3–D output sequence structure ([1x3x1] per timestep).

assessing the autoencoder performance(s). The 1st Convolutional hidden layer was used to extract the spatial input_features (normalized input sequence dataset) from the input layer. From the 1st hidden layer, the MaxPooling layer pools into its own network layer all the sequence data sample before passing through to subsequent convolutional hidden layer. Meanwhile, the time-distributed flatten layer was used to further narrow the output sequence array of the last convolutional hidden layer (layer 14) from the 4–D [1x3x1x1] to a 3–D output shape [1x3x1] before passing through to the reshape layer (decoder). The reshape layer extracts the wrapped input sequence samples from the time-distributed flatten layer and reshape (interpret) them for the autoencoder predictions before passing through to the output layer nodes with a 3–D output sequence structure ([1x3x1] per timestep).

A.2. GRU Autoencoding Architecture

The block diagram of the GRU autoencoding architecture in an unsupervised predictive operation was summarized in Fig S1. The GRU autoencoder was built with a 11–sequentially arranged network layer. For this model setup, a 3–D normalized input dataset with the noise signal was used as an input sequence

Table 7. Table 4a: Conv2D and GRU autoencoder metrics (CoD/MAE/RMSE) for the offshore noisy dataset (without noise removal)

Station	Model Type	WndDir			CNR			WndSpd		
IDS	Usage	(%)			(%)			(%)		
	......Conv2D............	CoD	MAE	RMSE	CoD MAE	RMSE	CoD	MAE	RMSE	
OST1	Prediction Conv2D_OST1	96.5	1.579	1.962	97.3 1.945	2.533	96.6	4.175	7.522	
OST3	Prediction Conv2D_OST3	99.0	1.381	1.657	98.7 1.729	2.226	98.0	4.065	7.367	
OST4	Prediction Conv2D_OST4	96.5	1.574	1.953	95.6 2.296	3.070	97.6	4.670	9.421	
		WndDir			CNR			WndSpd		
....	..............GRU..............	....	....	....	....			....		
	......Offshore...............	CoD	MAE	RMSE	CoD MAE	RMSE	CoD	MAE	RMSE	
OST1	Prediction GRU_OST1	95.8	1.685	3.237	98.5 1.756	2.147	79.9	6.686	13.179	
OST3	Prediction GRU_OST3	98.6	1.473	1.815	99.4 1.432	1.722	89.9	5.397	10.946	
OST4	Prediction GRU_OST4	98.4	1.509	1.839	95.6 2.258	2.186	97.6	4.095	7.470	

Table 8. Table 4b: Conv2D and GRU autoencoder metrics (CoD/MAE/RMSE) for the onshore noisy dataset (without noise removal)

| Station	Model Type	WndDir			Air_Temp			WndSpd		
IDs	Usage	(%)			(%)			(%)		
	.... Conv2D..............	CoD	MAE	RMSE	CoD MAE	RMSE	CoD	MAE	RMSE	
ST1	Prediction Conv2D_ST1	98.1	1.854	2.247	97.0 1.458	1.776	94.7	1.318	1.655	
ST3	Prediction Conv2D_ST3	99.2	1.283	1.517	98.3 1.433	1.749	97.4	1.303	1.566	
ST4	Prediction Conv2D_ST4	97.3	1.941	2.416	95.9 1.774	2.424	95.7	1.307	1.593	
		WndDir			Air_Temp			WndSpd		
....	..............GRU.............	....	....	....	....	....	....	....	....	
	.... Onshore.............	CoD	MAE	RMSE	CoD MAE	RMSE	CoD	MAE	RMSE	
ST1	Prediction GRU_ST1	98.5	1.236	1.443	97.2 1.249	1.462	97.4	1.281	1.496	
ST3	Prediction GRU_ST3	99.5	1.265	1.488	98.9 1.276	1.488	98.7	1.217	1.430	
ST4	Prediction GRU_ST4	98.7	1.218	1.471	96.8 1.440	1.868	98.2	1.228	1.483	
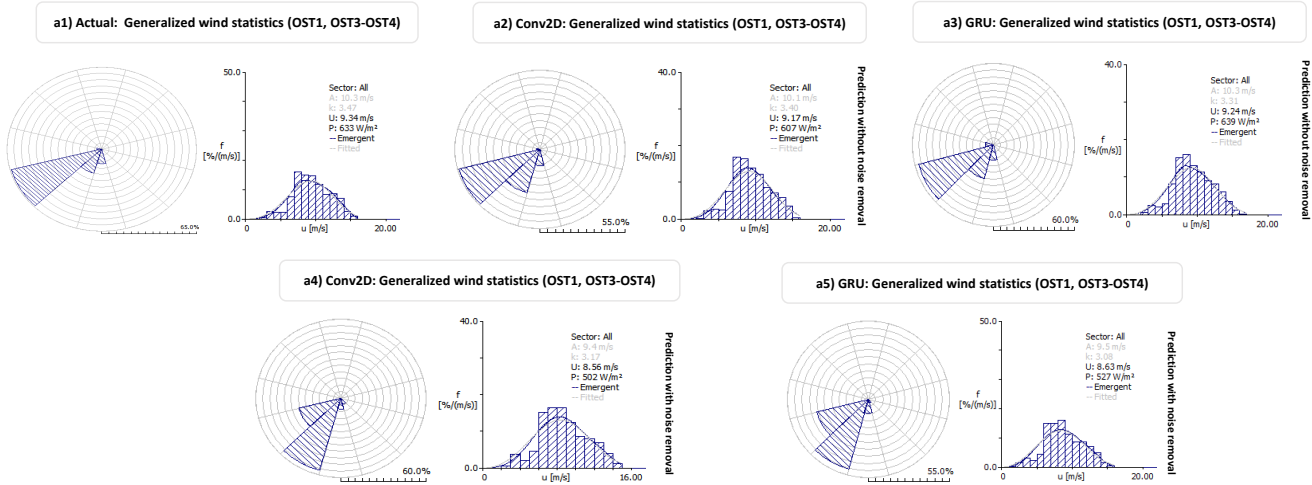
Fig. 18. Fig 15: aGeneralized wind statistics of combined 3-station heights (OST1, OST3-OST4); and b-doffshore wind statistics of each station height

A.3. 3-D/4-D Autoencoder Forecasts and Weibull Parameters

With the autoencoder framework in Section 3.3.1-3.3.2, the predictive systems with batch_data2 have been designed to make a reliable model forecast of the 3–station variables (3-output sequence [WndSpd, WndDir and 1CNR] for the offshore and [WndSpd, WndDir and 2Air Temperature] for the onshore) for the considered time period of 1008 (offshore station) and 1440 (onshore). With the new input sequence data of batch_data2 (A_io _Conv2D_noisy_pred for the investigated timesteps ($[t_1] - [t_{1008}]$) or/and A_io_GRU_noisy_pred for the investigated timesteps ($[t_1] - [t_{1440}]$), the station 3-variable forecasts (Col. 6 of Table 1a) were generated.

From the time-series predictions of the 1WndSpd and 2WndDir, the offshore/onshore wind resource statistics for individual station height were calculated from the actual, Conv2D and GRU predicted wind profiles in the WAsP software. From the time-series wind profile, the onshore/offshore wind power density using the Weibull distribution was calculated as follow:

$$P_W = \frac{1}{2}\rho(h)C^3\Gamma\left(1 + \frac{3}{k}\right) \quad \text{(14)}$$

where k, and C are the shape and scale parameters of the Weibull distribution, and PW is the Weibull wind power density.

A.4. Performance Evaluations of the Autoencoders

The performance of the two autoencoding models with an independent evaluation dataset of 5-residential buildings (Res-Ev1–Res-Ev5) was assessed. To measure the closeness (correlation) of the predicted station variable profiles to the actual datasets (baseline values), the forecast model skills were evaluated with the 4-quantitative metrics below:

$$CoD = \left\{\frac{\sum_{i=1}^{N}(A_{act_i} - \hat{A}_{act})(A_{pred_i} - \hat{A}_{pred})}{\sqrt{\sum_{i=1}^{N}((A_{act_i} - \hat{A}_{act})^2 \sum_{i=1}^{N}(A_{pred_i} - \hat{A}_{pred})^2)}}\right\}^2 * 100\%$$

$$\text{(15)}$$

$$MAE = \sum_{i=1}^{N}\frac{\left|A_{pred_i} - A_{act_i}\right|}{(N)} * 100\% \quad \text{(16)}$$

$$RMSE = \sqrt{\sum_{i=1}^{N}\frac{(A_{pred_i} - A_{act_i})^2}{(N)}} * 100\% \quad \text{(17)}$$

$$MSE = \sum_{i=1}^{N}\frac{(A_{pred_i} - A_{act_i})^2}{(N)} * 100\% \quad \text{(18)}$$

where $A_{pred,i}$ is the ith predicted values of the $A_{io\_conv2D\_pred}$ or $A_{io\_GRU\_pred}$ at any given timestep; A_{act} is the ith actual values of the station measurements; N is the total sample-size; CoD, MAE, RMSE and MSE are the estimated values of the correlation of determination, mean_absolute_error, root_mean_squared_error and mean_squared_error, respectively.

4. RESULTS AND DISCUSSION

A. Experimental Results

Experimental results of the autoencoder predicted multivariable profiles (WndSpd, WndDir, Air Temp and CNR) for each off-

Table 9. Table 4c: Improvement of the Conv2D and GRU autoencoder predictions without the feature noise removal over the model predictions with noise removal.

Station (IDs)	Model Type Usage	WndDir (%)			CNR (%)			WndSpd (%)		
	......Conv2D...............	ME	MAE	RMSE	ME MAE	RMSE		ME	MAE	RMSE
OST1	Prediction Conv2D_OST1	+25.4 %	+41.9 %	+23.7 %	+6.55 % +44.4%	+25.9%		+13.8%	+46.4 %	+28.3 %
OST3	Prediction Conv2D_OST3	+16.9 %	+42.3 %	+24.8 %	-0.027 % +49.9%	+8.7%		+8.7%	+46.1 %	+28.7 %
OST4	Prediction Conv2D_OST4	+31.5 %	+40.3 %	+23.9 %	+20.3% +38.7%	+21.8%		+13.6 %	+42.1 %	+24.0 %
		WndDir			CNR			WndSpd		
....	............GRU............	....	....	....	....	....	....	....	....	....
	......Offshore......	ME	MAE	RMSE	ME MAE	RMSE		ME	MAE	RMSE
OST1	Prediction GRU_OST1	+3.50 %	+46.9 %	+28.7 %	+7.89 % +45.9%	+25.9 %		+6.56 %	+43.4 %	+25.3 %
OST3	Prediction GRU_OST3	+3.10 %	+51.5 %	+33.8 %	+3.96 % +50.7%	+33.2 %		+4.23 %	+50.3 %	+33.1 %
OST4	Prediction GRU_OST4	-0.78 %	+53.5 %	+36.7 %	+4.77 % +49.1%	+31.8 %		-2.53 %	+53.5 %	+37.5 %

Table 10. Table 5: Summary of the best autoencoding architectures for 001-288 prediction timesteps

	Station	Heights (m)	Autoencoder Selection for WndDir	Autoencoder Selection for CNR	Autoencoder Selection for WndSpd
Offshore					
	OST1	73.8	Conv2D	GRU	Conv2D
	OST3	123.8	Conv2D	GRU	Conv2D
	OST4	153.8	GRU	GRU	GRU
	——	——	——	——	——
Onshore	Heights (m)		for WndDir	for Air_Temp	for WndSpd
	ST1	20	GRU	GRU	GRU
	ST3	20	GRU	GRU	GRU
	ST4	10	GRU	GRU	GRU

Table 11. Table 6: Summary of the dominant sectorwise wind directions for the autoencoder predictions and actual wind model (001-288 steps)

	Station Heights (m)	Actual Wind Rose	Conv2D Autoencoder Wind Rose without Noise Removal	GRU Autoencoder Wind Rose without Noise Removal	Conv2D Autoencoder Wind Rose with Noise Removal	GRU Autoencoder Wind Rose with Noise Removal
Offshore						
OST1	73.8	WSW	WSW	WSW	SSW	SSW
OST3	123.8	WSW	WSW	WSW	SSW	SSW
OST4	153.8	WSW	WSW	WSW	SSW	SSW
Onshore	———	————	————	————	————	————
ST1	20	SSW & WSW	WSW	SSW & WSW	SSW & WSW	SSW
ST3	20	WSW & W	WSW & W	WSW & W	WSW	WSW
ST4	10	W & WNW	W & WSW	W & WNW	WSW & W	WSW & W

Table 12. Table 7: Conv2D and GRU autoencoder evaluation results in terms of estimated MAE (%) and MSE (%) for the offshore and onshore stations.

| Station IDs	Model Type Usage	—— Res-Ev1	—— Res-Ev2	Conv2D Res-Ev3	—— Res-Ev4	Model Type Usage	—— Res-Ev1	—— Res-Ev2	GRU Res-Ev3	—— Res-Ev4
....	OFFSHORE	....	....	MAE (%)	....	OFFSHORE	....	....	MAE (%)	....
OST1	Evaluated Conv2D -OST1	18.70	18.96	32.42	31.73	Evaluated GRU -OST1	22.45	24.36	35.52	32.52
OST3	Evaluated Conv2D -OST3	20.54	19.90	33.87	31.47	Evaluated GRU -OST3	25.17	23.39	35.69	33.13
OST4	Evaluated Conv2D OST4	26.81	22.90	34.98	30.27	Evaluated GRU -OST4	23.27	20.45	32.41	29.53
....	OFFSHORE	....	....	MSE(%)	....	OFFSHORE	....	....	MSE (%)	....
OST1	Evaluated Conv2D -OST1	5.380	6.240	18.83	14.94	Evaluated GRU -OST1	7.410	9.770	19.06	16.98
OST3	Evaluated Conv2D -OST3	6.800	6.480	19.65	16.23	Evaluated GRU -OST3	10.33	8.130	20.07	16.35
OST4	Evaluated Conv2D -OST4	10.55	7.260	18.90	15.37	Evaluated GRU -OST4	7.870	6.660	18.37	13.27
Station IDs	Model Type Usage	—— Res-Ev1	—— Res-Ev2	Conv2D Res-Ev3	—— Res-Ev4	Model Type Usage	—— Res-Ev1	—— Res-Ev2	GRU Res-Ev3	—— Res-Ev4
....	ONSHORE	....	....	MAE (%)	....	ONSHORE	....	....	MAE (%)	....
ST1	Evaluated Conv2D -ST1	23.62	23.98	38.63	33.36	Evaluated GRU -ST1	20.83	22.01	38.48	30.09
ST3	Evaluated Conv2D -ST3	24.12	22.79	38.19	31.47	Evaluated GRU -ST3	22.03	20.72	37.26	29.47
ST4	Evaluated Conv2D -ST4	44.45	31.41	45.27	19.59	Evaluated GRU -ST4	44.38	31.30	34.18	18.87
....	ONSHORE	....	....	MSE(%)	....	ONSHORE	....	....	MSE (%)	....
ST1	Evaluated Conv2D -ST1	7.75	9.42	24.03	15.46	Evaluated GRU -ST1	6.37	8.02	22.70	14.05
ST3	Evaluated Conv2D -ST3	9.78	7.30	22.50	14.09	Evaluated GRU -ST3	7.55	6.02	21.61	13.19
ST4	Evaluated Conv2D -ST4	21.47	12.1	28.60	5.82	Evaluated GRU -ST4	21.08	11.94	19.24	5.36
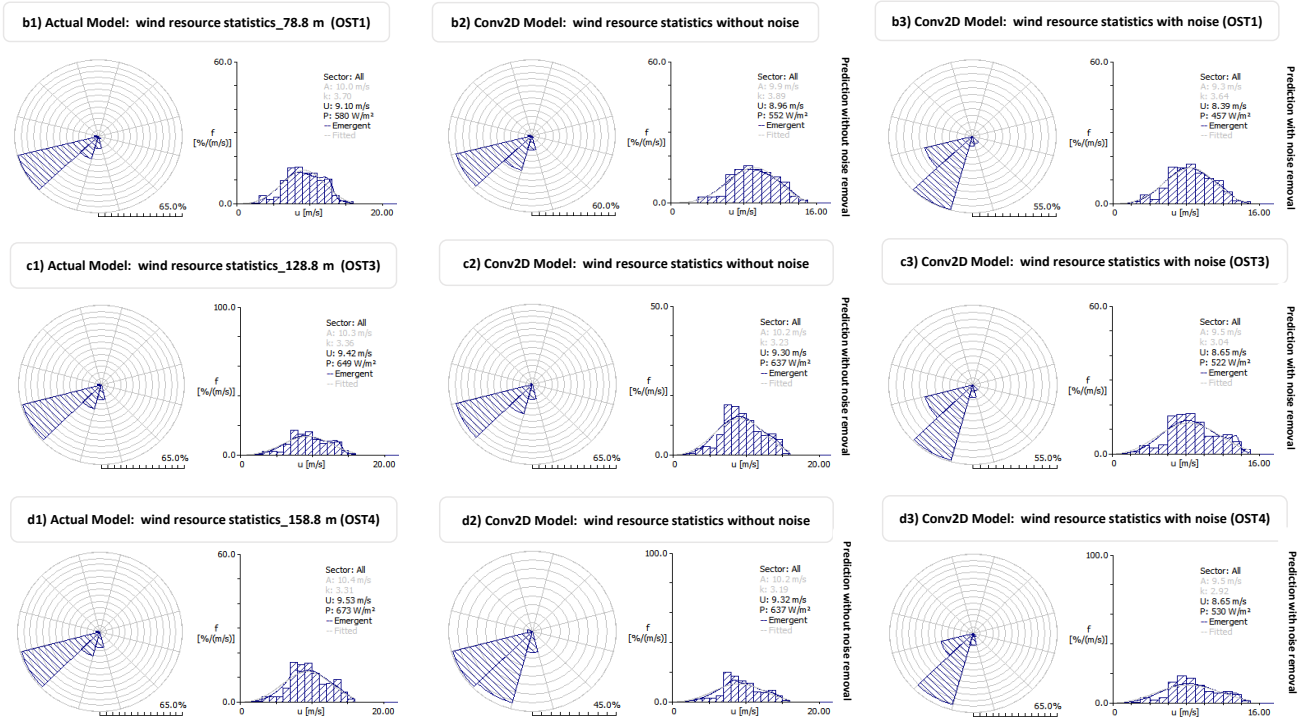
Fig. 19. Fig 15: aGeneralized wind statistics of combined 3-station heights (OST1, OST3-OST4); and b-doffshore wind statistics of each station height

shore and onshore station height as well as the actual profiles are all depicted in the Figs. 2–15, S2–S12 and Tables 2–7.

B. Discussion

B.1. Offshore wind profile comparisons (Conv2D vs. GRU)

For every sampling period of 48 timesteps, the time-series of the Conv2D autoencoder predictions for batch_data2 input sequences (model prediction dataset of Cols. 5 and 8 of Table 1b) have been compared with the actual profiles for each offshore station height (Figs 5–6 and S6). For the time-series predictions without the feature noise removal (data noise inclusion), the offshore wind speeds are compared with the actual measurements at 78.8 m height (Fig 5a). Also, the offshore wind speed predictions with the feature noise removal are compared (Fig. 5b). Furthermore, the time-series predictions of the offshore wind speeds for other station heights of 128.8 (Fig S6a) and 153.8 m (Fig S6b) are provided. As reported in Fig. 6, the time-series predictions of the offshore wind direction with and without the noise removal are compared with the actual measurements of 78.8 m height (OST1). Moreover, the plots of the predicted CNR values with and without the data noise removal are compared with the time-series of the actual CNR measurements (Fig 7).

For the total period of 288 timesteps, the multi-variable actual profiles of the offshore station 'WndSpd, WndDir and CNR' are well reproduced by the two autoencoding models (Conv2D and GRU) as the introduction of the feature noise signal with the batch_data2 input dataset did enhance the overall performance of the considered models. Although, the time-series predictions (3–variable model outputs) of the Conv2D autoencoders with the feature noise signal removal (Fig. b of 5–7) for OST1 (78.8 m

height) show the: - 1close (similar) trend with the actual measurement and 2slight improvement over the model output (time-series predictions) without the feature nose removal (Fig a of 5–7), however, the plots of the Conv2D wind roses revealed that its more appropriate to assess the sectorwise wind flow using the Conv2D predictions without the feature noise removal (Fig 8i). Additionally, the similar studied findings for the Conv2D predicted wind roses for other offshore station heights of 128.8 m (Fig 8ii) and 153.8 m (Fig 8iii) are reported. In a similar development, the graphs of the GRU predicted wind roses without and with the feature noise removal of the offshore station heights of 73.8 m (Fig c and e of 8i), 128.8 m (Fig c and e of 8ii) and 158.8 m (Fig c and e of 8iii) are compared to the: - Conv2D predicted wind roses without and with the noise removal (Fig b and d of 8i–8iii) and the actual wind roses (Fig a of 8i–8iii). The dominant sectorwise wind flows from the Conv2D and GRU model predictions with and without noise removal, as well as the actual wind flows for the total sampling period of 288 timesteps are summarized (Table 6). In similar to the Conv2D predicted wind roses without the noise removal (Fig b of 8i-8ii), we observed that the GRU model predicted wind roses without the noise removal (Fig c of 8i–8iii) strongly aligned with the actual wind roses (Fig a of 8i–8iii). For the model forecast periods of 1–288 timesteps, the figurative comparisons of the GRU (Fig e of 8i–8iii) and the Conv2D (Fig d of 8i–8iii) predicted wind roses with the data noise removal revealed that our two autoencoding architectures with the noise removal technique was a misrepresentation (Table 4c) of the actual wind flows (Fig 8a) for the considered offshore station heights. Based on the sectorwise wind flows for the similar forecast period, the best autoencoder for assessing each offshore station variable (WndSpd, WndDir

and CNR) is depicted in Table 5. At the OST1 and OST3 station heights, the Conv2D autoencoder appears to be more suitable for assessing the offshore wind profiles (WndDir and WndSpd) only while the GRU autoencoder is found to be more reliable for the CNR assessment of the OST1 and OST3. At OST4 only, the GRU autoencoder appears to be more reliable for assessing all the station 3–variables (rows 2–4 of Table 5) as compared to the Conv2D autoencoder suitability.

Finally, the frequency distributions of the Conv2D and GRU predicted wind flows without the noise removal (Figs b1–b2 of 9–10 and S7) are compared to: 1the frequency distributions of the Conv2D and GRU predicted wind flows with the noise removal (Figs. c1–c2 of 9–10 and S7) as well as 2the frequency distributions of the actual wind flows. For the dominant actual wind flows in the WSW direction (Col. 3 of Table 6), the Conv2D and GRU model frequency distributions without the noise removal recorded a close-tie with the actual frequency distributions (Figs. a of 9–10 and S7) for all sectorwise directions (o) of the offshore wind speeds (m/s).
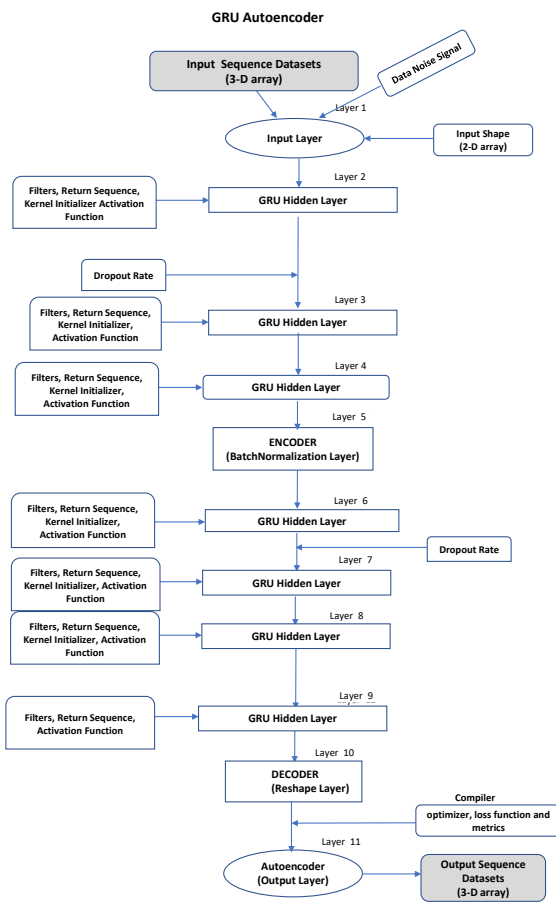
Fig S1: Block Diagram of a GRU Autoencoder (Unsupervised Predictive System)

Fig. 20. FS1: Block Diagram of a GRU Autoencoder (Unsupervised Predictive System)

B.2. Onshore wind profile comparisons (Conv2D vs. GRU)

The time-series of the Conv2D wind profiles for each station height are compared with the Actual wind profiles (Fig. 11) of the similar sampling period of 48 timesteps. For the Conv2D autoencoder predictions without (Fig 11a) and with the feature noise removal (Fig 11b), the onshore wind speeds at ST1 are summarized and compared with the actual wind speed measurement of 20 m height. Additionally, the offshore wind directions without (Fig. 11c) and with (Fig. 11d) the noise removal are compared with the actual measurements of 20 m height at ST1. Furthermore, the time-series predictions of the onshore wind speeds of 20 m height at ST3 (Fig. S9a) and of 10 m height at ST4 (Fig. S9b) are compared with their actual wind measurements. Further to this, the plot of the Air_Temp without (Fig S8a) and with the feature noise removal (Fig S8b) are compared with the actual values. With the new input sequence datasets (prediction datasets in Cols. 5 and 8 of Table 1b) for the total period of 288 timesteps, the time-series of the actual profiles of the onshore station multi-variables [WndSpd, WndDir, Air_Temp] are well captured/reproduced by the our autoencoders (Conv2D and GRU models). Also, the comparison study reveals that the introduction of the feature noise signal into the station variable datasets (model input data) did enhanced greatly the overall performance of the autoencoders for the time-series multivariate predictions. The Conv2D time-series predictions (model outputs) with the feature noise removal for ST1 (Figs. 11b, 11d and S8b) recorded a closer trend with the actual values as compared to the Conv2D predictions without the noise removal (Figs 11a, 11c and S8a). Also, the Conv2D predicted wind roses without and with the noise removal (Figs. b and d of 12i) revealed that its more appropriate to assess the sectorwise wind directions with the noise removal (Fig d of 12i) than to assess the sectorwise wind direction with the noisy dataset/without the noise removal (Fig b of 12i). Nevertheless, a similar study is carried out also for ST3 at 20 m (Fig 12i) and ST4 at 10 m heights (Fig S11i). The studied finding reveals that the Conv2D and GRU model outputs without the noise removal at ST3 (Fig b-c of 12ii) are more appropriate for assessing the sectorwise wind directions (wind rose) while the GRU model outputs without the feature noise removal at ST4 is more appropriate for assessing the sectorwise wind directions/flows (Fig c of S11i). In the similar develop-
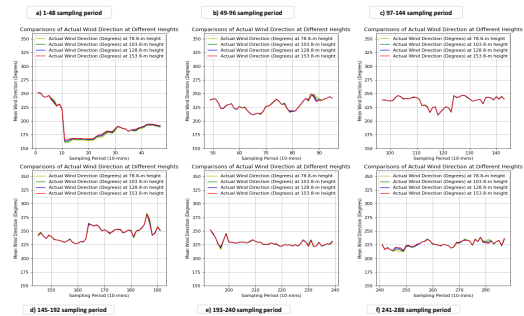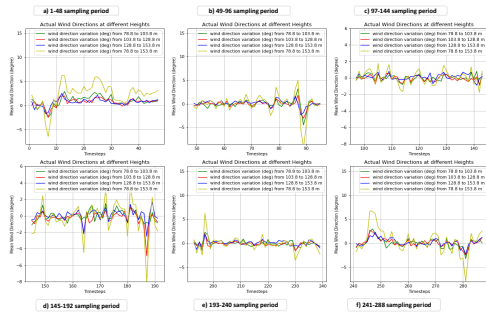

Fig. 21. FS2: Time-series of actual offshore wind directions (degrees) at different measured heights (OST1-OST4)

ment, the GRU model wind roses at an onshore height of ST1 (Fig c and e of 12i), ST3 (Fig c and e of 12ii) and ST4 (Fig c and e of S11i) have been compared with the Conv2D wind roses (Figs. b and d of 12i–12ii and S11i) and the actual wind roses (Figs. a

of 12i–12ii and S11i). Meanwhile, the dominant sectorwise wind flows of the Conv2D and GRU autoencoders are compared also with the actual wind roses (Table 6). Similar to the Conv2D wind roses with the noise removal (Fig d of 12i), the GRU wind rose without the noise removal (Fig c of 12i) strongly agrees with the actual wind rose (Fig a of 12i) at ST1. For a similar period of 288 timesteps, 1the GRU wind rose with a noise removal (Fig e of 12i) and the Conv2D wind rose without the noise removal (Fig b of 12i) at ST1; 2the GRU wind rose with noise removal (Fig e of 12ii) and the Conv2D wind rose with the noise removal (Fig d of 12ii) at ST3; and the 3GRU wind rose with noise removal (Fig e of S11i), Conv2D wind rose with a noise removal (Fig d of S11i) and Conv2D wind rose without the noise removal (Fig b of S11i) at ST4 are all poor representations of the actual wind flow at the considered onshore stations (Table 6). Based on the sectorwise wind flows for a period of 1–288 timesteps, the best autoencoder for assessing each onshore station variable (Wnd-Dir/CNR/WndSpd) is depicted in Table 5. At ST1, ST3 and ST4, the GRU autoencoder is seen to be more suitable for assessing all the onshore station multi-variables (WndDir, Air_Temp and WndSpd) as compared to the Conv2D autoencoder (rows 6–8 of Table 5). Finally, the frequency distributions of the Conv2D

Fig. 22. FS3: Time-series of actual offshore wind direction variations (degree) at different measured heights (OST1 - OST4)

and GRU wind profiles without the feature noise removal (Figs b1–b2 of 13–14 and S12) are compared to the frequency distributions with the noise removal (Figs. c1–c2 of 13–14 and S12). For the dominant wind flows in the SSW&WSW (ST1), WSW&W (ST3), W&WNW (ST4) direction (Col 3 of Table 6), the studied findings show that the GRU model frequency distribution without the feature noise removal (Figs. b2 of 13–14 and S12) are closer to the actual frequency distributions (Figs. 13a, 14a and S12a) in all sectorwise wind directions (o). In comparisons of the predicted with the actual model wind, the generalized wind statistics of the combined 3-station heights (OST1, OST3 and OST4) of Fig 15a revealed that the offshore wind statistics of the GRU model without the feature noise removal could be used as a stand-alone forecast model in analyzing the time-series of the wind profiles of a particular climatic zone.

B.3. Autoencoders forecast metrics

The predictive skill of each autoencoder is assessed by measuring the reliability of the offshore and onshore forecasts in terms of model: 1deviation from and 2connectivity with the actual (baseline) values. From the forecast horizons of 1-288 timesteps, the estimated model errors (MAE and RMSE) and the forecast accuracy (CoD) of each autoencoder in the offshore time-series multivariable prediction have been analysed (Table
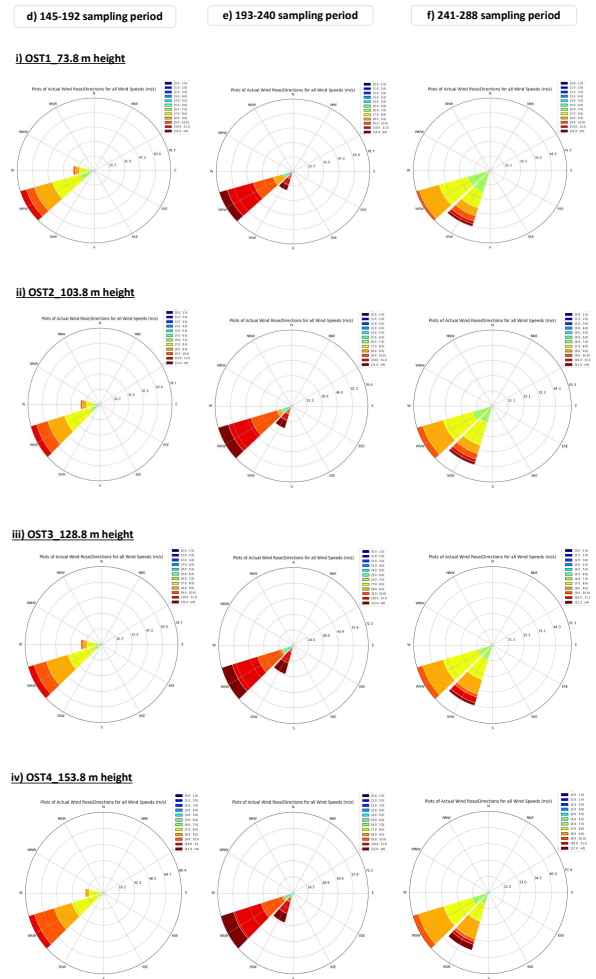

Fig. 23. FS4: Actual model comparisons of offshore wind roses at different measured heights (OST1 - OST4)

4a-b). Furthermore, the improvements of the Conv2D and GRU autoencoder predictions without the feature noise removal over the same model predictions with the feature noise removal are compared in Table 4c. From the model comparative results of the Conv2D and GRU autoencoders (Table 4a) with the actual value, the Conv2D reported the highest CoD with the lowest MAE and RMSE values for the time-series predictions of the WndDir and WndSpd at OST1 and OST3 station heights; while the GRU reported the highest CoD with the lowest MAE and RMSE values for the predictions of the WndDir and WndSpd at OST4 height. Notwitstanding, the GRU autoencoder recorded the highest CoD with the lowest MAE and RMSE values for the CNR time-series predictions of all the offshore heights (OST1, OST3 and OST4). For the onshore station heights (ST1, ST3 and ST4) of Table 4b, the GRU model reported the highest CoD with the lowest MAE and RMSE values for all the predicted station multi-variables (WndDir, WndSpd and Air_Temp) at the ST1, ST3 and ST4. In general, the Conv2D autoencoder in the assessment of the offshore station variables of the WndDir and WndSpd of the OST1 and OST3 shows superiority over the
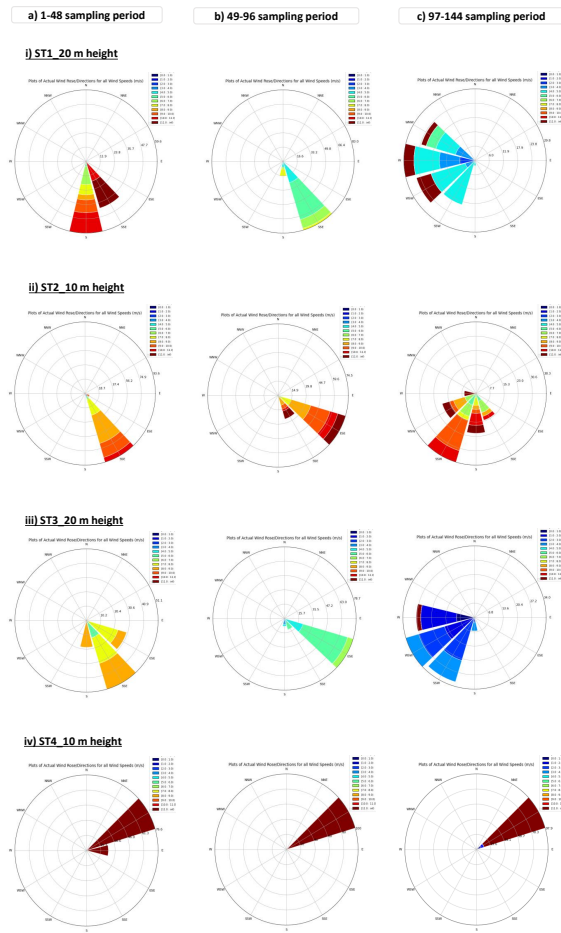
Fig. 24. FS5a: Actual model comparisons of onshore wind roses (001-144 timesteps) at different station masts (ST1 - ST4)

Fig. 25. FS5b: Actual model comparisons of onshore wind roses (145-288 timesteps) at different station masts (ST1 - ST4)

other autoencoder metrics, with exception to the station variable of CNR where the GRU autoencoder shows its superiority over the Conv2D. Nevertheless, the GRU autoencoder in the time-series prediction of the onshore station multivariables of the ST1/ST2/ST3 shows its superiority over the Conv2D autoencoder metrics. The predictive skills of each autoencoder for the offshore and onshore stations are evaluated with independent energy building datasets (Res-Ev1–Res-Ev5) of Table 1c. In Table 7, the model evaluated results of the Conv2D and GRU autoencoders in term of the estimated MSE and MAE values have been depicted. For the evaluated Conv2D and GRU autoencoders of each offshore/onshore height, the model skill scores (MAE and MSE) comparison reveals that a single autoencoding architecture (Conv2D) is insufficient and unrealible for assessing all the offshore multi-variables from the height of OST1–OST4 while the evaluated skill scores for the onshore stations reveal that a single autoencoding architecture (GRU) is sufficient for assessing of all the station multivariables from the heights of ST1–ST4. Generally, these evaluated model results (Table 7) strongly agreed with the best predicted model
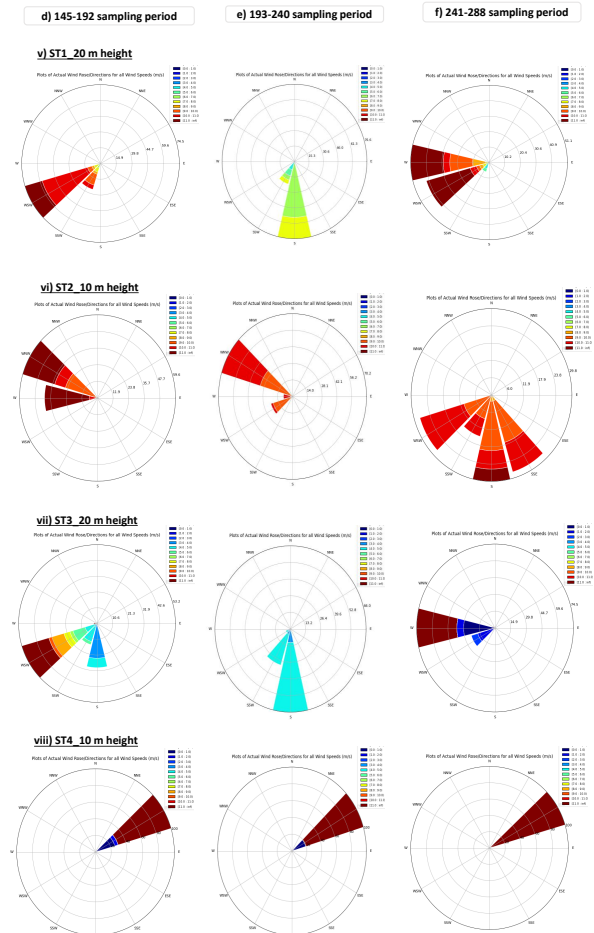
skills reported in Tables 4a-b and 5, respectively. Lastly, in finding the baseline forecast architecture for the 1description of the wind variability (non-linear forecast solutions) and 2analysis of the time-series of the offshore and onshore wind profiles for a particular climatic zone, our forecast metrics of the Conv2D and GRU autoencoders are compared with the CNN and LSTM autoencoder metrics reported by Chandra et al [54]. Our autoencoder forecast skills in the multi-step variable predictions are better off when compared to Chandra investigated LSTM and ED-LSTM forecast models (Tables 4-11). To estabilish the superiority of our autoencoder skills over other forecast model performances reported in other literature, the estimated MAE and RMSE values of our presented models are compared to the SVM and LSTM model performances of Pallonetto et al [72]. Pallonetto et al reported MAE (kW) and RMSE (%) values of 12.642 and 3.54 for the LSTM, 11.539 and 3.26, respectively for the SVM (Table 2); while our summarized hourly forecast errors in Table 4a-b are lower. Also, the power consumption forecast accuracy (CoD=0.772 and MAE=0.314) of the CNN and the supply capacity prediction skill (CoD=0.336 and MAE=0.479) of the
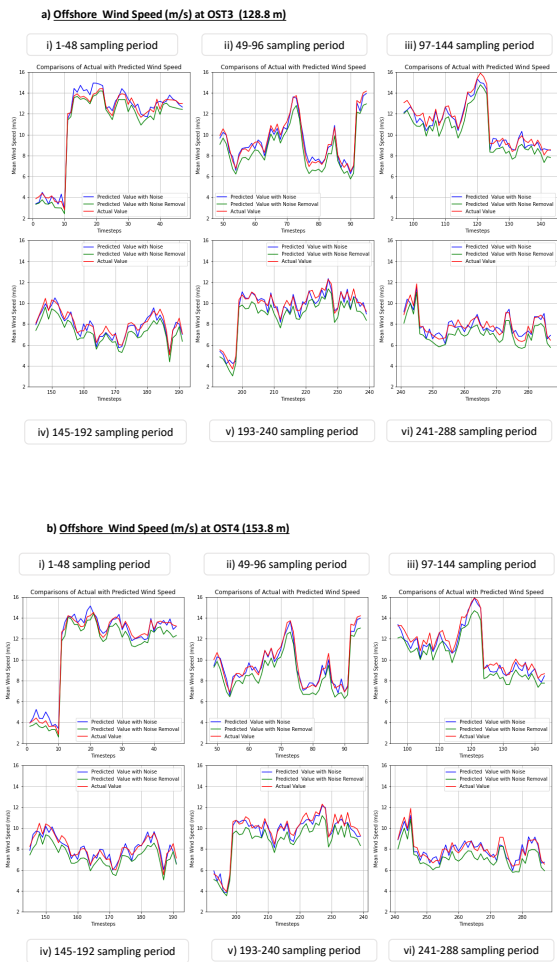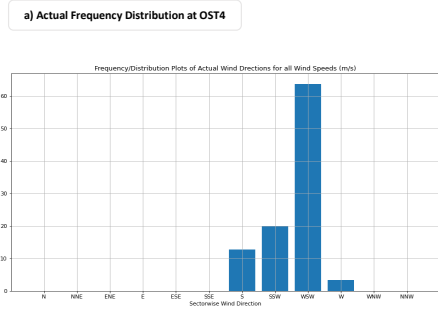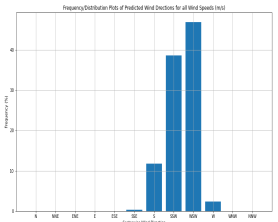
a) Offshore Wind Speed (m/s) at OST3 (128.8 m)

i) 1-48 sampling period   ii) 49-96 sampling period   iii) 97-144 sampling period

iv) 145-192 sampling period   v) 193-240 sampling period   vi) 241-288 sampling period

b) Offshore Wind Speed (m/s) at OST4 (153.8 m)

i) 1-48 sampling period   ii) 49-96 sampling period   iii) 97-144 sampling period

iv) 145-192 sampling period   v) 193-240 sampling period   vi) 241-288 sampling period

a) Actual Frequency Distribution at OST4

b1) Conv2D: Predicted Frequency Distribution without Noise Removal   **b2) GRU: Predicted Frequency Distribution without Noise Removal**
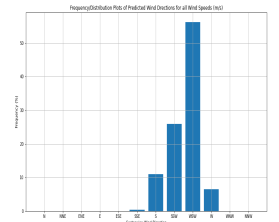
c1) Conv2D: Predicted Frequency Distribution with Noise Removal   **c2) GRU: Predicted Frequency Distribution with Noise Removal**

Fig. 26. FS6: Actual and Conv2D autoencoder plots of offshore wind speeds (m/s) at OST3-OST4, respectively

Fig. 27. FS7: Actual, Conv2D and GRU model comparisons of frequency distribution of offshore wind speeds (m/s) at OST4

hybrid (CNN and RNN) models of Kang et al [73] are compared to the Conv2D and GRU model forecast scores of our presented study (see Table 4). The estimated values of CoD and MAE of our considered autoencoders outperformed the CoD and MAE values of their models. Lastly, our high forecast skills of Conv2D and GRU autoencoders are compared to the Yongsheng et al [74] reported ELM model score (RMSE: 3.678–5.817) as well as Gensler et al [75] reported autoencoder and conventional LSTM skills (Auto-LSTM RMSE = 7.13%). Although, theYongsheng et al and Gensler et al model skills within the context of solar forecasting were considered, however, our model performance for the multivariate predictions outperformed the investigated model of Yongsheng et al [74], motivating the general use of our autoencoding architecture as the baseline forecast model in : 1. describing the wind variability (non-linear forecast solutions) and 2. analysing the wind speed/direction profiles of a particular climatic zone.
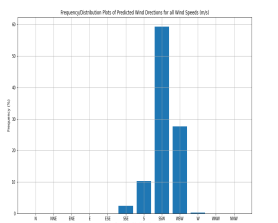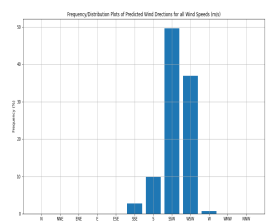
5. CONSLUSION

The development of an autoencoding predictive model plays a vital role in describing the variability of the long-term offshore and onshore multivariable profiles of a particular climatic zone. Based on our selected temporal resolutions of the historical multivariate input sequence obtained from the two different geographical zones, the analysis of the offshore and onshore station multivariables at 8-different heights have been considered with 2-different autoencoding models in an unsupervised predictive operation. Based on the comparison of the model predictions with the actual measurements, the analysis and comparison of the: 1time-series and sectorwise wind profiles, 2CNR and 3prevailing air temperatures have been carried out. The experimental findings of the analysis of the offshore wind speed-direction at 4–different heights revealed that the lidar station height was driven by weather condition impacts, with the steadiest offshore wind flows recorded above 128.8 m height (OST3–OST4) as compared to the other station heights of 78.8–103.8, 103.8–128.8 and 78.8–153.8 m. Also, our experimental findings revealed that the
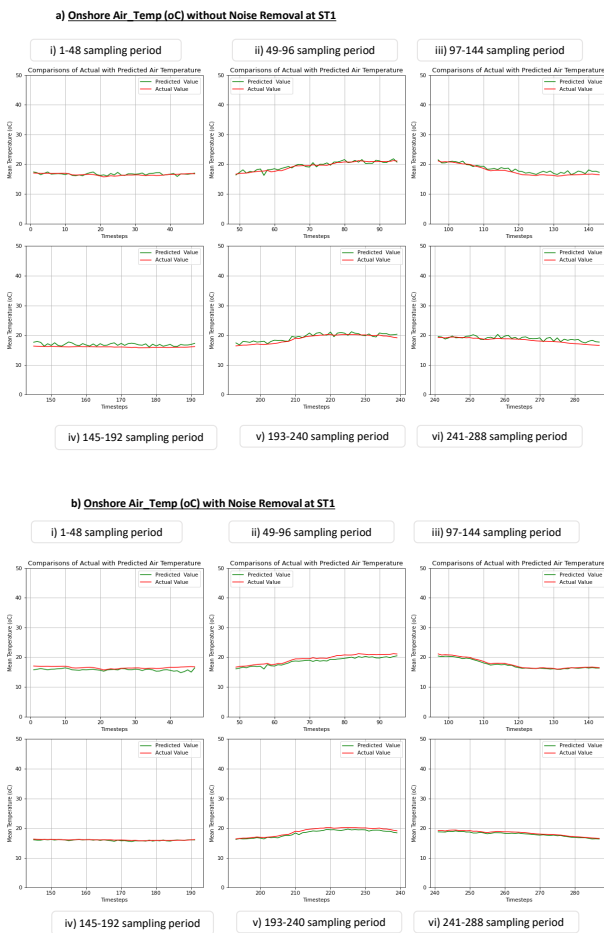
Fig. 28. FS8: Actual and Conv2D autoencoder plots of onshore Air_Temp (oC) with and without noise removal at ST1

Fig. 29. FS9: Conv2D autoencoder plots of time-series of onshore wind speeds (m/s) at ST3 and ST4, respectively

dominant wind flows at the onshore (ST1–ST4) in all the sectorwise wind directions vary for each station height and were greatly impacted by their local surface irregularity. Thus, the analysed wind profiles of each onshore station height (ST1–ST4) required that the wind flows be modelled as a function of the atmospheric conditions or/and local effects (topographic description of the site) while the offshore wind flow above 128.8 m height is more suitable for an optimal loading of the WET. The importance and superiority of the GRU and Conv2D autoencoders in the time-series predictions and analysis of the station multivariables have been observed. Upon the evaluation of our considered autoencoders, we suggest that the presented autoencoder architectures were essential tools for assessing the time-series multivariables at 5–min/10–min intervals for two different geographical zones. Finally, the comparison results of the autoencoder frequency distribution of the offshore and onshore wind profiles with and without the feature noise elimination have proven that the GRU autoencoder produced a better forecast and was a better choice for the analysis of the time-series of the station multivariables (WndDir, Air_Temp and WndSpd) at
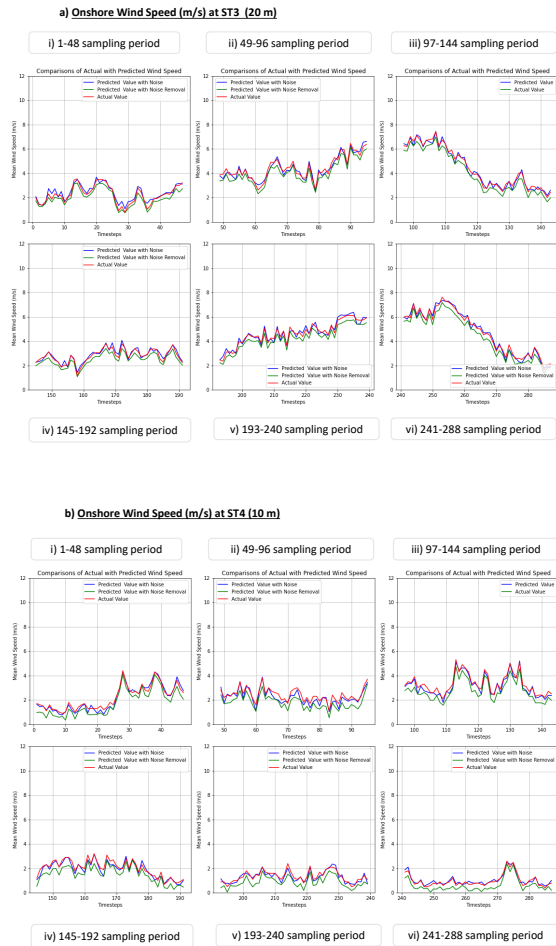
the onshore heights, while the Conv2D and GRU autoencoders were needful for an accurate assessment of the time-series of the offshore multivariables (WndDir, CNR and WndSpd). The use of the Conv2D autoencoder only didn't improve the overall prediction and evaluation accuracy scores of each offshore height. Regardless of this, implementing the 2-autoencoding models with the presented feature noise technique for the time-series prediction of the multivariables did not only improve the reliability of the ML models in the long-term (offshore and onshore) wind forecasting, but also provide the more robust wind resource estimates for the considered station height. Sequel to this, our experimental findings are summarized:

- The two investigated autoencoding architectures (Conv2D and GRU) in the analysis of the hourly wind profiles of both the offshore and onshore heights are needful, while a single autoencoder (GRU) architecture is needful for the analysis of the time-series profiles of the onshore multivariate input features.

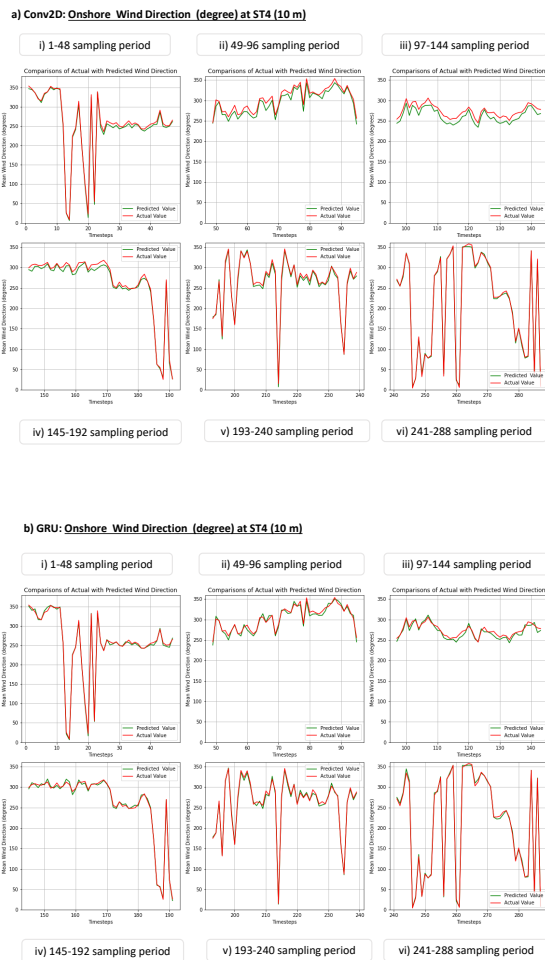- The Conv2D autoencoder with a combination of the off-

Fig. 30. FS10: Conv2D and GRU autoencoder plots of onshore wind directions with noise (degree) at ST4, respectively

Fig. 31. FS11: Actual, Conv2D and GRU autoencoder comparisons of onshore wind roses at ST4 (1-288 steps)

term multivariable forecasting from 1-288 horizons, and the analysis of the: wind speed and direction, sectorwise windrose, CNR and prevailing air temperature at a given offshore and onshore station height. Also, the introduction of the feature noise technique significantly impacted the autoencoder learning of the non-linear dynamics of the multivariate input data sequence.

Competing interests
The authors declare that no competing interests (financially or technically) exist.

Authors' contributions and Acknowledgements
The research method description with the historical dataset processing as well as the paper presentation was designed and written by the Author. The Author is grateful for the part-funded of ZakkWea Energy towards this research work.

shore station datasets of 78.8–158.8 m heights produced the generalized model score errors (ME = 0.105 m/s and RMSE = 0.420 m/s for the WndSpd; ME = -3.10 and RMSE = 6.20 for WndDir) while the GRU model score errors (ME = 0.019 m/s and RMSE = 0.396 m/s for WndSpd; ME = -2.90 and RMSE = 7.90 for the WndDir) are reported for the autoencoder predictions without the feature noise removal. Without the feature noise removal, the generalised offshore wind statistics of the Conv2D and GRU architectures for the combination of 3–station height datasets (OST1 and OST3–OST4) exhibit the similar wind trends (patterns) with the generalised offshore wind statistics from the Actual model, while the superiority of the Conv2D model over the GRU architecture was recorded for the estimated offshore wind statistics of individual station height (OST1/OST3/OST4).

- Lastly, the sequentially arranged layers of the considered Conv2D and GRU autoencoders (3–D input sequence and 3–D output sequence structure) made it ideal for a long-
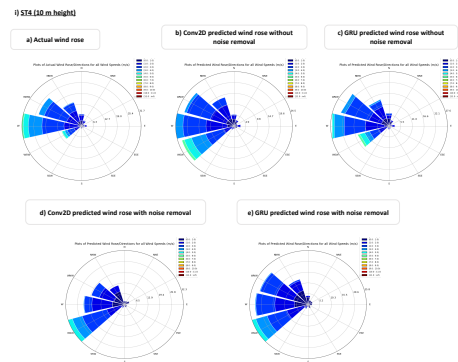
REFERENCES

1. E. López, C. Valle, H. Allende, E. Gil, and H. Madsen, "Wind power forecasting based on echo state networks and long short-term memory," *Energies*, vol. 11, no. 3, p. 526, 2018.
2. B. C. G. De Aguiar and M. J. S. Valença, "Using reservoir computing for forecasting of wind power generated by a wind farm," in *Proceedings of the Sixth International Conference on Advanced Cognitive Technologies and Applications, Venice, Italy*, pp. 25–29, Citeseer, 2014.
3. M. Drechsler, J. Egerer, M. Lange, F. Masurowski, J. Meyerhoff, and M. Oehlmann, "Efficient and equitable spatial allocation of renewable power plants at the country scale," *Nature Energy*, vol. 2, no. 9, pp. 1–9, 2017.
4. M. R. Shaner, S. J. Davis, N. S. Lewis, and K. Caldeira, "Geophysical constraints on the reliability of solar and wind power in the united states," *Energy & Environmental Science*, vol. 11, no. 4, pp. 914–925, 2018.
5. R. E. Abdel-Aal, "Hourly temperature forecasting using abductive networks," *Engineering Applications of Artificial Intelligence*, vol. 17, no. 5, pp. 543–556, 2004.
6. J. Cifuentes, G. Marulanda, A. Bello, and J. Reneses, "Air temperature forecasting using machine learning techniques: a review," *Energies*, vol. 13, no. 16, p. 4215, 2020.
7. G. Mihalakakou, M. Santamouris, and A. Tsangrassoulis, "On the energy consumption in residential buildings," *Energy and buildings*, vol. 34, no. 7, pp. 727–736, 2002.
8. Ö. A. Dombaycı and M. Gölcü, "Daily means ambient temperature prediction using artificial neural network method: A case study of turkey," *Renewable Energy*, vol. 34, no. 4, pp. 1158–1161, 2009.
9. A. Camia, G. Bovio, I. Aguado, and N. Stach, "Meteorological fire danger indices and remote sensing," *Remote Sensing of Large Wildfires: in the European Mediterranean Basin*, pp. 39–59, 1999.
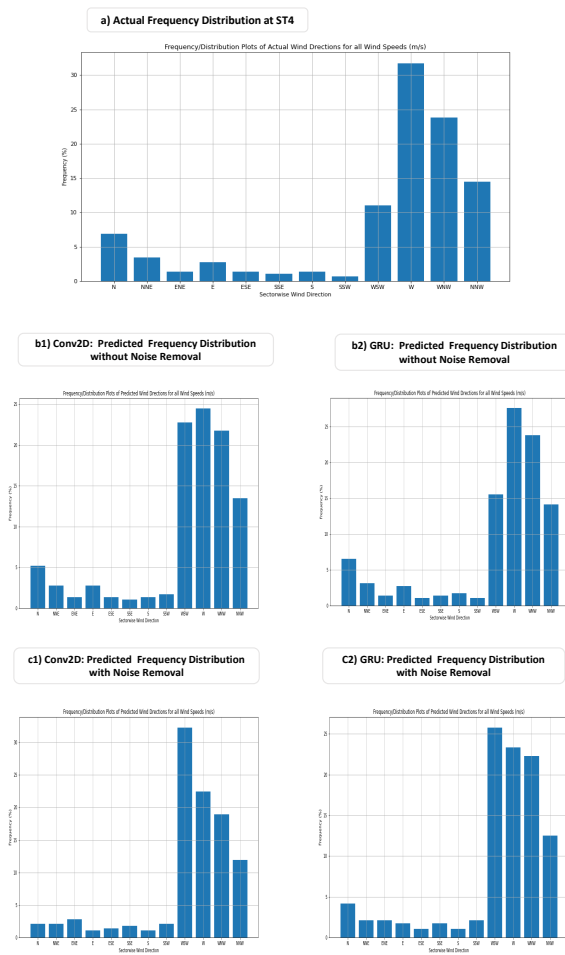
Fig. 32. FS12: Actual, Conv2D and GRU model comparisons of frequency distribution of onshore wind speeds (m/s) at ST4

2022.

16. A. Alkesaiberi, F. Harrou, and Y. Sun, "Efficient wind power prediction using machine learning methods: A comparative study," *Energies*, vol. 15, no. 7, p. 2327, 2022.

17. Y. Mao and W. Shaoshuai, "A review of wind power forecasting & prediction," in *2016 International Conference on probabilistic methods applied to power systems (PMAPS)*, pp. 1–7, IEEE, 2016.

18. N. A. Treiber, J. Heinermann, and O. Kramer, "Wind power prediction with machine learning," *Computational sustainability*, pp. 13–29, 2016.

19. T. Matsumoto and M. Endo, "One-week-ahead electricity price forecasting using weather forecasts, and its application to arbitrage in the forward market: An empirical study of the japan electric power exchange," *Journal of Energy Markets*, vol. 14, no. 3, 2021.

20. L. M. Giordano and D. Morale, "A fractional brownian–hawkes model for the italian electricity spot market: estimation and forecasting," *arXiv preprint arXiv:1911.11795*, 2019.

21. D. Schönheit, C. Dierstein, D. Möst, and L. Lorenz, "Zone-wide prediction of generating unit-specific power outputs for electricity grid congestion forecasts," *Journal of Energy Markets*, vol. 14, no. 2, 2020.

22. Z. Hu, C. Li, Y. Cao, B. Fang, L. He, and M. Zhang, "How smart grid contributes to energy sustainability," *Energy Procedia*, vol. 61, pp. 858–861, 2014.

23. T. Logenthiran, D. Srinivasan, and A. M. Khambadkone, "Multi-agent system for energy resource scheduling of integrated microgrids in a distributed system," *Electric Power Systems Research*, vol. 81, no. 1, pp. 138–148, 2011.

24. V. N. Coelho, M. W. Cohen, I. M. Coelho, N. Liu, and F. G. Guimarães, "Multi-agent systems applied for energy systems integration: State-of-the-art applications and trends in microgrids," *Applied energy*, vol. 187, pp. 820–832, 2017.

25. I. Akhtar, S. Kirmani, and M. Jameel, "Reliability assessment of power system considering the impact of renewable energy sources integration into grid with advanced intelligent strategies," *IEEE Access*, vol. 9, pp. 32485–32497, 2021.

26. D. Tong, D. J. Farnham, L. Duan, Q. Zhang, N. S. Lewis, K. Caldeira, and S. J. Davis, "Geophysical constraints on the reliability of solar and wind power worldwide," *Nature communications*, vol. 12, no. 1, p. 6146, 2021.

27. H. Holttinen, A. Tuohy, M. Milligan, E. Lannoye, V. Silva, S. Müller, L. Sö, *et al.*, "The flexibility workout: managing variable resources and assessing the need for power system modification," *IEEE Power and Energy Magazine*, vol. 11, no. 6, pp. 53–62, 2013.

28. W. Dong and S. Li, "Reliability sensitivity of wind power system considering correlation of forecast errors based on multivariate nstpnt method," *Protection and Control of Modern Power Systems*, vol. 6, no. 1, pp. 1–11, 2021.

29. M. A. Hossain, R. K. Chakrabortty, S. Elsawah, and M. J. Ryan, "Very short-term forecasting of wind power generation using hybrid deep learning model," *Journal of Cleaner Production*, vol. 296, p. 126564, 2021.

30. H. Madsen, H. A. Nielsen, and T. S. Nielsen, "A tool for predicting the wind power production of off-shore wind plants," in *Proceedings of the Copenhagen Offshore Wind Conference & Exhibition*, 2005.

31. S. Al-Deen, A. Yamaguchi, T. Ishihara, and R. Bessa, "A physical approach to wind speed prediction for wind energy forecasting," *Journal of Wind Engineering*, vol. 108, pp. 349–352, 2006.

32. W.-Y. Chang *et al.*, "A literature review of wind forecasting methods," *Journal of Power and Energy Engineering*, vol. 2, no. 04, p. 161, 2014.

33. F. Cassola and M. Burlando, "Wind speed and wind energy forecast through kalman filtering of numerical weather prediction model output," *Applied energy*, vol. 99, pp. 154–166, 2012.

34. S. Al-Deen, A. Yamaguchi, T. Ishihara, and R. Bessa, "A physical approach to wind speed prediction for wind energy forecasting," *Journal of Wind Engineering*, vol. 108, pp. 349–352, 2006.

35. T. Ishihara, A. Yamaguchi, and Y. Fujino, "A nonlinear model mascot: development and application," in *Proc. of 2003 European Energy Conference and Exhibition*, vol. 1, pp. 1–7, 2003.

36. L. Li, Y.-q. Liu, Y.-p. Yang, H. Shuang, and Y.-m. Wang, "A physical

10. S. Malakar, S. Goswami, B. Ganguli, A. Chakrabarti, S. S. Roy, K. Boopathi, and A. Rangaraj, "Designing a long short-term network for short-term forecasting of global horizontal irradiance," *SN Applied Sciences*, vol. 3, pp. 1–15, 2021.

11. M. A. García and J. Balenzategui, "Estimation of photovoltaic module yearly temperature and performance based on nominal operation cell temperature calculations," *Renewable energy*, vol. 29, no. 12, pp. 1997–2010, 2004.

12. D. M. Smith, S. Cusack, A. W. Colman, C. K. Folland, G. R. Harris, and J. M. Murphy, "Improved surface temperature prediction for the coming decade from a global climate model," *science*, vol. 317, no. 5839, pp. 796–799, 2007.

13. "World meteorological organization," *Available online: https://public.wmo.int/en/our-mandate/what-we-do (accessed on 1 February 2019)*, 2019.

14. A. E. Ben-Nakhi and M. A. Mahmoud, "Cooling load prediction for buildings using general regression neural networks," *Energy Conversion and Management*, vol. 45, no. 13-14, pp. 2127–2141, 2004.

15. S. C. Nwokolo, J. C. Ogbulezie, and A. U. Obiwulu, "Impacts of climate change and meteo-solar parameters on photosynthetically active radiation prediction using hybrid machine learning with physics-based models," *Advances in Space Research*, vol. 70, no. 11, pp. 3614–3637,

approach of the short-term wind power prediction based on cfd pre-calculated flow fields," *Journal of Hydrodynamics, Ser. B*, vol. 25, no. 1, pp. 56–61, 2013.

37. L. Landberg, "Short-term prediction of local wind conditions," *Journal of Wind Engineering and Industrial Aerodynamics*, vol. 89, no. 3-4, pp. 235–245, 2001.

38. U. Focken, M. Lange, and H.-P. Waldl, "Previento-a wind power prediction system with an innovative upscaling algorithm," in *Proceedings of the European Wind Energy Conference, Copenhagen, Denmark*, vol. 276, 2001.

39. Y. Liu, M. C. Roberts, and R. Sioshansi, "A vector autoregression weather model for electricity supply and demand modeling," *Journal of Modern Power Systems and Clean Energy*, vol. 6, no. 4, pp. 763–776, 2018.

40. M.-D. Wang, Q.-R. Qiu, and B.-W. Cui, "Short-term wind speed forecasting combined time series method and arch model," in *2012 International Conference on Machine Learning and Cybernetics*, vol. 3, pp. 924–927, IEEE, 2012.

41. H. Liu, H.-Q. Tian, C. Chen, and Y.-f. Li, "A hybrid statistical method to predict wind speed and wind power," *Renewable energy*, vol. 35, no. 8, pp. 1857–1861, 2010.

42. E. Cadenas, W. Rivera, R. Campos-Amezcua, and C. Heard, "Wind speed prediction using a univariate arima model and a multivariate narx model," *Energies*, vol. 9, no. 2, p. 109, 2016.

43. R. R. De Aquino, R. B. Souza, O. N. Neto, M. M. Lira, M. A. Carvalho, and A. A. Ferreira, "Echo state networks, artificial neural networks and fuzzy systems models for improve short-term wind speed forecasting," in *2015 International Joint Conference on Neural Networks (IJCNN)*, pp. 1–8, IEEE, 2015.

44. W. Sun, M. Liu, and Y. Liang, "Wind speed forecasting based on feemd and lssvm optimized by the bat algorithm," *Energies*, vol. 8, no. 7, pp. 6585–6607, 2015.

45. Q. Wu and C. Peng, "Wind power generation forecasting using least squares support vector machine combined with ensemble empirical mode decomposition, principal component analysis and a bat algorithm," *Energies*, vol. 9, no. 4, p. 261, 2016.

46. F. Bonanno, G. Capizzi, G. L. Sciuto, and C. Napoli, "Wavelet recurrent neural network with semi-parametric input data preprocessing for micro-wind power forecasting in integrated generation systems," in *2015 International Conference on Clean Electrical Power (ICCEP)*, pp. 602–609, IEEE, 2015.

47. D. Liu, J. Wang, and H. Wang, "Short-term wind speed forecasting based on spectral clustering and optimised echo state networks," *Renewable Energy*, vol. 78, pp. 599–608, 2015.

48. C. Sheng, J. Zhao, Y. Liu, and W. Wang, "Prediction for noisy nonlinear time series by echo state network based on dual estimation," *Neurocomputing*, vol. 82, pp. 186–195, 2012.

49. Z. Zhao, W. Chen, X. Wu, P. C. Chen, and J. Liu, "Lstm network: a deep learning approach for short-term traffic forecast," *IET Intelligent Transport Systems*, vol. 11, no. 2, pp. 68–75, 2017.

50. S. Brusca, G. Capizzi, G. Lo Sciuto, and G. Susi, "A new design methodology to predict wind farm energy production by means of a spiking neural network–based system," *International Journal of Numerical Modelling: Electronic Networks, Devices and Fields*, vol. 32, no. 4, p. e2267, 2019.

51. A. S. Devi, G. Maragatham, K. Boopathi, and A. Rangaraj, "Hourly day-ahead wind power forecasting with the eemd-cso-lstm-efg deep learning technique," *Soft Computing*, vol. 24, no. 16, pp. 12391–12411, 2020.

52. P. Lu, L. Ye, W. Zhong, Y. Qu, B. Zhai, Y. Tang, and Y. Zhao, "A novel spatio-temporal wind power forecasting framework based on multi-output support vector machine and optimization strategy," *Journal of Cleaner Production*, vol. 254, p. 119993, 2020.

53. R. Chandra, S. Goyal, and R. Gupta, "Evaluation of deep learning models for multi-step ahead time series prediction," *IEEE Access*, vol. 9, pp. 83105–83123, 2021.

54. Y. LeCun, Y. Bengio, and G. Hinton, "Deep learning," *nature*, vol. 521, no. 7553, pp. 436–444, 2015.

55. X. Chen, X. Zhang, M. Dong, L. Huang, Y. Guo, and S. He, "Deep learning-based prediction of wind power for multi-turbines in a wind farm," *Frontiers in Energy Research*, vol. 9, p. 723775, 2021.

56. S. C. Nwokolo, S. O. Amadi, A. U. Obiwulu, J. C. Ogbulezie, and E. E. Eyibio, "Prediction of global solar radiation potential for sustainable and cleaner energy generation using improved angstrom-prescott and gumbel probabilistic models," *Cleaner Engineering and Technology*, vol. 6, p. 100416, 2022.

57. S. C. Nwokolo, A. U. Obiwulu, J. C. Ogbulezie, and S. O. Amadi, "Hybridization of statistical machine learning and numerical models for improving beam, diffuse and global solar radiation prediction," *Cleaner Engineering and Technology*, vol. 9, p. 100529, 2022.

58. A. Sagheer and M. Kotb, "Unsupervised pre-training of a deep lstm-based stacked autoencoder for multivariate time series forecasting problems," *Scientific reports*, vol. 9, no. 1, p. 19038, 2019.

59. W. Bao, J. Yue, and Y. Rao, "A deep learning framework for financial time series using stacked autoencoders and long-short term memory," *PloS one*, vol. 12, no. 7, p. e0180944, 2017.

60. N. Shabbir, L. Kütt, M. Jawad, O. Husev, A. U. Rehman, A. A. Gardezi, M. Shafiq, and J.-G. Choi, "Short-term wind energy forecasting using deep learning-based predictive analytics," *Comput. Mater. Contin*, vol. 72, pp. 1017–1033, 2022.

61. C. Huang, H. R. Karimi, P. Mei, D. Yang, and Q. Shi, "Evolving long short-term memory neural network for wind speed forecasting," *Information Sciences*, vol. 632, pp. 390–410, 2023.

62. U. Cali and V. Sharma, "Short-term wind power forecasting using long-short term memory based recurrent neural network model and variable selection," *Int. J. Smart Grid Clean Energy*, vol. 8, no. 2, pp. 103–110, 2019.

63. T. Anushalini and B. Sri Revathi, "Role of machine learning algorithms for wind power generation prediction in renewable energy management," *IETE Journal of Research*, pp. 1–14, 2023.

64. C. Fu, G.-Q. Li, K.-P. Lin, and H.-J. Zhang, "Short-term wind power prediction based on improved chicken algorithm optimization support vector machine," *Sustainability*, vol. 11, no. 2, p. 512, 2019.

65. J. Wang, H. Zhu, Y. Zhang, F. Cheng, and C. Zhou, "A novel prediction model for wind power based on improved long short-term memory neural network," *Energy*, vol. 265, p. 126283, 2023.

66. D. Zhang, X. Peng, K. Pan, and Y. Liu, "A novel wind speed forecasting based on hybrid decomposition and online sequential outlier robust extreme learning machine," *Energy conversion and management*, vol. 180, pp. 338–357, 2019.

67. A. Kumar and A. S. Ali, "Prospects of wind energy production in the western fiji—an empirical study using machine learning forecasting algorithms," in *2017 Australasian Universities Power Engineering Conference (AUPEC)*, pp. 1–5, IEEE, 2017.

68. S. Sun, Y. Liu, Q. Li, T. Wang, and F. Chu, "Short-term multi-step wind power forecasting based on spatio-temporal correlations and transformer neural networks," *Energy Conversion and Management*, vol. 283, p. 116916, 2023.

69. H. Demolli, A. S. Dokuz, A. Ecemis, and M. Gokcek, "Wind power forecasting based on daily wind speed data using machine learning algorithms," *Energy Conversion and Management*, vol. 198, p. 111823, 2019.

70. "Anholt and westermost rough lidar data documentation,"

71. S. Ong and N. Clark, "Commercial and residential hourly load profiles for all tmy3 locations in the united states," tech. rep., DOE Open Energy Data Initiative (OEDI); National Renewable Energy Lab.(NREL . . . , 2014.